14% in *RAD51B*$^{+/-/-/-}$ cells (Table 1). The expression of the *RAD51B* cDNA in the mutant reduced the frequency of such aberrations to 5%. Similarly, in metaphase, the frequency was 6% in WT cells, 13.5% in *RAD51B*$^{+/+/-/-}$ cells, and 25.5% in *RAD51B*$^{+/-/-/-}$ cells. The expression of the *RAD51B* cDNA in the mutant reduced the frequency to 10.5%. Thus, haploinsufficiency of *RAD51B* leads to increased centrosome fragmentation.

***RAD51B* haploinsufficiency leads to increased aneuploidy.** Extra centrosome-like structures can unequally distribute chromosomes to daughter cells, which is thought to cause aneuploidy. We therefore examined the frequency of aneuploidy by fluorescence *in situ* hybridization (FISH) using two independent chromosome-specific centromere probes (Fig. 4*C*; Table 2). At chromosome 7, the frequencies of aneuploidy represented by one or three signals were 5.4% in WT cells, whereas the corresponding frequency was 9.8% in *RAD51B*$^{+/+/-/-}$ cells and 14% in *RAD51B*$^{+/-/-/-}$ cells. At chromosome 17, the frequencies of aneuploidy were 3.8% in WT cells, whereas the corresponding frequency was 7.4% in *RAD51B*$^{+/+/-/-}$ cells and 10.2% in *RAD51B*$^{+/-/-/-}$ cells. The differences between WT cells and the mutant cells were statistically significant ($P < 0.05$, Fisher's exact test). Expression of the *RAD51B* cDNA in the mutant reduced the frequency of aneuploidy to 6.4% at chromosome 7 and 4.2% at chromosome 17 ($P < 0.05$). Thus, haploinsufficiency of *RAD51B* leads to increased aneuploidy.

Table 1. Distribution of centrosome numbers

Cell line	1 or 2	3	4	>4	% Abnormality
Interphase					
HCT116					
RAD51B$^{+/+/+/+}$	190	8	2	0	5
RAD51B$^{+/+/-/-}$	177	15	7	1	11.5
RAD51B$^{+/-/-/-}$	172	22	4	2	14
RAD51B$^{+/-/-/-}$ + *RAD51B*	190	8	1	1	5
HT1080					
Control siRNA	197	1	2	0	1.5
RAD51B siRNA	192	6	2	0	4
Metaphase					
HCT116					
RAD51B$^{+/+/+/+}$	188	11	1	0	6
RAD51B$^{+/+/-/-}$	173	22	4	1	13.5
RAD51B$^{+/-/-/-}$	149	41	10	0	25.5
RAD51B$^{+/-/-/-}$ + *RAD51B*	179	19	2	0	10.5
HT1080					
Control siRNA	195	3	2	0	2.5
RAD51B siRNA	167	26	7	0	16.5

NOTE: A total of 200 cells were scored for each line.

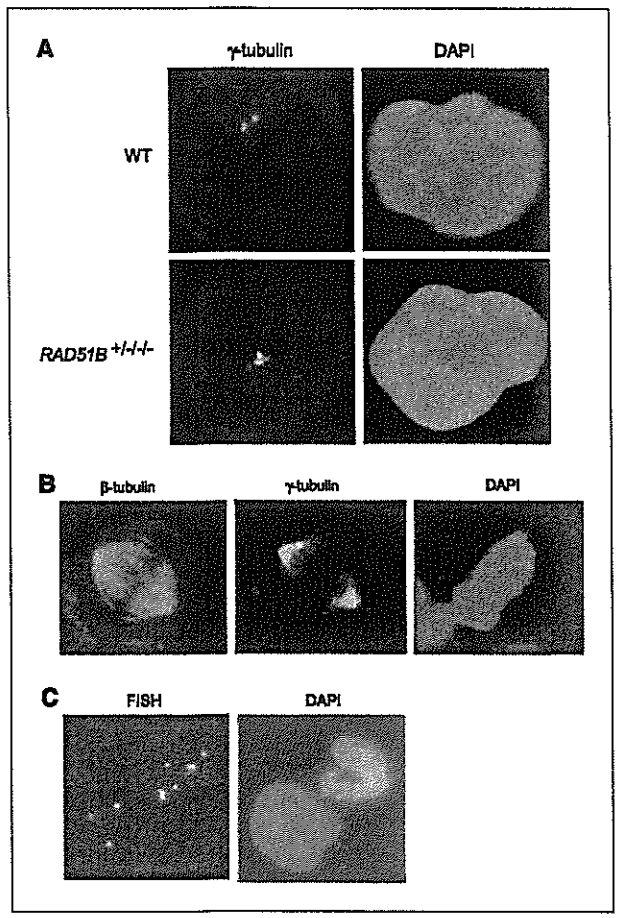

Figure 4. Centrosome fragmentation and aneuploidy in the *rad51b*-mutant cells. *A*, interphase *RAD51B*$^{+/-/-/-}$ cell with multiple centrosomes. *DAPI*, 4′,6-diamidino-2-phenylindole. *B*, metaphase *RAD51B*$^{+/-/-/-}$ cell showing multiple centrosomes and bipolar spindles. *C*, FISH on *RAD51B*$^{+/-/-/-}$ cells using a probe for chromosome 7 (*orange*) and a probe for chromosome 17 (*green*).

It is possible that *RAD51B*$^{+/-/-/-}$ cells will acquire more copies of the WT allele and form significant subpopulations due to increased aneuploidy. To investigate this possibility, we examined a difference in *RAD51B* expression levels between originally isolated cells and cells passaged 25 times by Northern blot analysis and found no difference. Thus, despite the problem of chromosome segregation, the *RAD51B*$^{+/-/-/-}$ status is stable.

A reduction in *RAD51B* levels leads to centrosome fragmentation in HT1080 cells. To confirm that a reduction in *RAD51B* levels leads to centrosome fragmentation in other human cells, we knocked down the gene in HT1080 cells by small interfering RNA (siRNA) transfection. Real-time PCR analysis revealed that the mRNA ratio of *RAD51B*/*GAPDH* was $2.5 \pm 0.6 \times 10^{-4}$ (mean ± SD; $n = 3$) in cells transfected with a control vector, whereas it was $1.2 \pm 0.1 \times 10^{-4}$ in cells transfected with a Rad51B knockdown vector. Thus, an ~50% reduction in *RAD51B* mRNA levels was achieved by RNAi. The frequency of aberrant numbers of interface centrosomes was 1.5% in cells transfected with the control vector, whereas it was 4% in cells transfected with the *RAD51B* knockdown vector (Table 1). In metaphase, the frequency was 2.5% in the control cells and 16.5% in *RAD51B* knockdown cells. Thus, like the haploinsufficiency of *RAD51B* in HCT116 cells, the 50% reduction in *RAD51B* mRNA levels in HT1080 cells leads to centrosome fragmentation.

Discussion

In the present study, we have shown that haploinsufficiency of *RAD51B* leads to centrosome fragmentation and increased aneuploidy in the human cancer cell line HCT116. In addition,

we have confirmed that Rad51B plays a role in homologous recombination repair in concert with Rad51 in human cells, which is consistent with the previous finding in DT40 cells (22). However, the absence of *RAD51B* haploinsufficiency in knockout mice and DT40 mutants may argue against this interpretation of the findings (22, 23). This apparent discrepancy may be the result of species differences and/or differences between cell types. One finding of the present study, that a 50% reduction in *RAD51B* mRNA levels by RNAi in HT1080 cells also leads to centrosome fragmentation, suggests that the effects of *RAD51B* haploinsufficiency may not be specific to HCT116 cells. Furthermore, the present findings are also supported by evidence of haploinsufficiency for *XRCC2* in mouse cells (40). *XRCC2*$^{+/-}$ mice and *XRCC2*$^{+/-}$ DT40 cells have been shown to exhibit no apparent abnormalities (37, 41), whereas haploinsufficiency for the gene was clearly observed in chromosome aberrations and centrosome fragmentation in *XRCC2*$^{+/-}$ mouse embryonic fibroblasts. Rad51B forms a complex with Rad51C, Rad51D, and XRCC2 (BCDX2), suggesting a functional similarity between these Rad51 paralogues (42, 43). These subtle effects of haploinsufficiency on genomic instability, even if they are much weaker than the effects of homozygous mutations, are likely to be of considerable importance in carcinogenesis when they confer a growth advantage.

Although centrosome aberrations have been observed in cells defective in other recombination genes, the molecular mechanisms underlying these aberrations are unclear. Centrosome amplification has been shown to arise from a DNA damage-induced mechanism during the prolonged G_2 phase in Rad51-deficient DT40 cells (14). Deletion of ATM reduced, but did not completely abolish, G_2-phase centrosome amplification, thus indicating ATM-dependent and ATM-independent mechanisms. However, a recent study using CHO cells argues against this interpretation (44).

Centrosome aberrations found in cells deficient in a member of the Rad51 paralogue family seem to be centrosome fragmentations (13, 15). A recent observation has indicated that centrosomes split into fractions containing only one centriole, which leads to the formation of multipolar spindles with extra centrosome-like structures in the presence of incompletely replicated or damaged DNA during mitosis (45). This result is also observed in CHO cells deficient in XRCC3, suggesting that aneuploidy in this cell line arises from extra centrosome-like structures. It is therefore possible that centrosome fragmentation resulting from haploinsufficiency of *RAD51B* could be explained by centrosome splitting.

Table 2. Distribution of chromosome numbers

Cell line	1	2	3	4	>4	1 + 3
Chromosome 7						
RAD51B$^{+/+/+/+}$	17	469	10	4	0	27
RAD51B$^{+/+/-/-}$	27	442	22	8	1	49
RAD51B$^{+/-/-/-}$	52	419	18	9	2	70
RAD51B$^{+/-/-/-}$ + *RAD51B*	18	465	14	3	0	32
Chromosome 17						
RAD51B$^{+/+/+/+}$	16	476	3	5	0	19
RAD51B$^{+/+/-/-}$	23	452	14	10	1	37
RAD51B$^{+/-/-/-}$	37	439	14	9	1	51
RAD51B$^{+/-/-/-}$ + *RAD51B*	17	478	4	1	0	21

NOTE: A total of 500 cells were scored for each line.

Aneuploidy is a hallmark of genetic instability observed in human cancers, although the direct cause remains a matter of debate (46). Extra centrosome-like structures are likely to lead to the assembly of multipolar spindles, which may in turn lead to the unequal distribution of chromosomes to daughter cells. However, supernumerary centrosomes do not always result in multipolarity, as shown by a recent finding that dynein plays a role in the prevention of multipolar spindles by centrosomal clustering (47). Consistent with this finding, multipolar spindles are rarely detected in the *rad51b* mutant, despite the increase in the incidence of supernumerary centrosomes. It is therefore unlikely that multipolar spindles play a causal role in increased aneuploidy in this mutant. This raises the question of how supernumerary centrosomes lead to aneuploidy. A possible clue may come from the characterization of the practical consequences of centrosome amplification in *p53*$^{-/-}$ mouse embryo fibroblasts (48, 49). In cells with two centrosomes at one spindle pole, a small fraction of chromosomes can be bioriented between incompletely separated centrosomes. Although these cells may divide in a bipolar fashion, this abnormal mitosis is likely to lead to the loss or gain of a few chromosomes.

From the viewpoint of tumor biology, it is of great importance that at least one allele of *RAD51B* is altered in some benign tumors, although the key pathologic alteration is still unclear. It is noteworthy that functional domains of Rad51B, such as Walker A and B motifs, are often lost as a consequence of the chromosome translocation, in contrast to the translocation partner HMGA2, the coding region of which is not rearranged by the translocation (28). It is well established that benign tumors do not usually develop into malignant tumors. However, a small proportion of benign tumors transforms into malignant tumors; <1% of uterine leiomyomas progress into uterine sarcomas. Given that the chromosome translocation involving *RAD51B* results in the loss of one functional *RAD51B* allele, the present finding that haploinsufficiency of the gene leads to aneuploidy implies chromosome instability in tumors harboring these translocations. The present study indicates that *rad51b*-mutant cells grow at a slightly slower rate than WT cells, implying that centrosome fragmentation and aneuploidy are not directly linked to a growth advantage. Aneuploidy is likely to contribute to a growth advantage only when genes that control cell growth are altered by the accumulation of chromosome instabilities. These observations lead to the hypothesis that the haploinsufficiency of *RAD51B*, even if not directly linked to malignant transformation, may play a role in the early steps of tumor development by inducing chromosome instability. To verify this hypothesis, a detailed analysis of *RAD51B* in association with pathologic and clinical studies in tumors involving 14q23-24 will be needed.

Acknowledgments

Received 8/8/2005; revised 3/16/2006; accepted 4/13/2006.

Grant support: Ministry of Education, Culture, Sports, Science, and Technology of Japan; Ministry of Health, Labour, and Welfare of Japan; and Hiroshima University 21st Century Center of Excellence Program (M. Katsura and T. Yoshihara).

The costs of publication of this article were defrayed in part by the payment of page charges. This article must therefore be hereby marked *advertisement* in accordance with 18 U.S.C. Section 1734 solely to indicate this fact.

References

1. Delattre M, Gonczy P. The arithmetic of centrosome biogenesis. J Cell Sci 2004;117:1619–29.
2. Lingle WL, Barrett SL, Negron VC, et al. Centrosome amplification drives chromosomal instability in breast tumor development. Proc Natl Acad Sci U S A 2002;99:1978–83.
3. Pihan GA, Purohit A, Wallace J, Malhotra R, Liotta L, Doxsey SJ. Centrosome defects can account for cellular and genetic changes that characterize prostate cancer progression. Cancer Res 2001;61:2212–9.
4. Fukasawa K, Choi T, Kuriyama R, Rulong S, Vande Woude GF. Abnormal centrosome amplification in the absence of p53. Science 1996;271:1744–7.
5. Harvey M, Sands AT, Weiss RS, et al. *In vitro* growth characteristics of embryo fibroblasts isolated from p53-deficient mice. Oncogene 1993;8:2457–67.
6. Tutt A, Gabriel A, Bertwistle D, et al. Absence of Brca2 causes genome instability by chromosome breakage and loss associated with centrosome amplification. Curr Biol 1999;9:1107–10.
7. Zhou H, Kuang J, Zhong L, et al. Tumour amplified kinase *STK15/BTAK* induces centrosome amplification, aneuploidy, and transformation. Nat Genet 1998;20:189–93.
8. Pastink A, Eeken JCJ, Lohman PHM. Genomic integrity and the repair of double-strand DNA breaks. Mutat Res 2001;480-481:37–50.
9. Valerie K, Povirk LF. Regulation and mechanisms of mammalian double-strand break repair. Oncogene 2003;22:5792–812.
10. West SC. Molecular views of recombination proteins and their control. Nat Rev Mol Cell Biol 2003;4:435–45.
11. Xu X, Weaver Z, Linke SP, et al. Centrosome amplification and a defective G_2-M cell cycle checkpoint induce genetic instability in BRCA1 exon 11 isoform-deficient cells. Mol Cell 1999;3:389–95.
12. Yamaguchi-Iwai Y, Sonoda E, Sasaki MS, et al. Mre11 is essential for the maintenance of chromosomal DNA in vertebrate cells. EMBO J 1999;18:6619–29.
13. Griffin CS, Simpson PJ, Wilson CR, Thacker J. Mammalian recombination-repair genes *XRCC2* and *XRCC3* promote correct chromosome segregation. Nat Cell Biol 2000;2:757–61.
14. Dodson H, Bourke E, Jeffers LJ, et al. Centrosome amplification induced by DNA damage occurs during a prolonged G_2 phase and involves ATM. EMBO J 2004;23:3863–73.
15. Smiraldo PG, Gruver AM, Osborn JC, Pittman DL. Extensive chromosomal instability in *Rad51d*-deficient mouse cells. Cancer Res 2005;65:2089–96.
16. Hsu L-C, White RL. BRCA1 is associated with the centrosome during mitosis. Proc Natl Acad Sci U S A 1998;95:12983–8.
17. Rice MC, Smith ST, Bullrich F, Havre P, Kmiec EB. Isolation of human and mouse genes based on homology to REC2, a recombinational repair gene from the fungus *Ustilago maydis*. Proc Natl Acad Sci U S A 1997;94:7417–22.
18. Sigurdsson S, Van Komen S, Bussen W, Schild D, Albala JS, Sung P. Mediator function of the human Rad51B-Rad51C complex in Rad51/RPA-catalyzed DNA strand exchange. Genes Dev 2001;15:3308–18.
19. Lio Y-C, Mazin AV, Kowalczykowski SC, Chen DJ. Complex formation by the human Rad51B and Rad51C DNA repair proteins and their activities *in vitro*. J Biol Chem 2003;278:2469–78.
20. Yokoyama H, Kurumizaka H, Ikawa S, Yokoyama S, Shibata T. Holliday junction binding activity of the human Rad51B protein. J Biol Chem 2003;278:2767–72.
21. Liu Y, Masson J-Y, Shah R, O'Regan P, West SC. RAD51C is required for Holliday junction processing in mammalian cells. Science 2004;303:243–6.
22. Takata M, Sasaki MS, Sonoda E, et al. The Rad51 paralog Rad51B promotes homologous recombinational repair. Mol Cell Biol 2000;20:6476–82.
23. Shu Z, Smith S, Wang L, Rice MC, Kmiec EB. Disruption of *muREC2/RAD51L1* in mice results in early embryonic lethality which can be partially rescued in a $p53^{-/-}$ background. Mol Cell Biol 1999;19:8686–93.
24. Thacker J. The *RAD51* gene family, genetic instability, and cancer. Cancer Lett 2005;219:125–35.
25. Schoenmakers EFPM, Huysmans C, Van de Ven WJM. Allelic knockout of novel splice variants of human recombination repair gene *RAD51B* in t(12;14) uterine leiomyomas. Cancer Res 1999;59:19–23.
26. Ingraham SE, Lynch RA, Kathiresan S, Buckler AJ, Menton AG. *hREC2*, a *RAD51*-like gene, is disrupted by t(12;14)(q15;q24.1) in a uterine leiomyoma. Cancer Genet Cytogenet 1999;115:56–61.
27. Takahashi T, Nagai N, Oda H, Ohama K, Kamada N, Miyagawa K. Evidence for *RAD51L1/HMGIC* fusion in the pathogenesis of uterine leiomyoma. Genes Chromosomes Cancer 2001;30:196–201.
28. Quade BJ, Weremowicz S, Neskey DM, et al. Fusion transcripts involving *HMGA2* are not a common molecular mechanism in uterine leiomyomata with rearrangements in 12q15. Cancer Res 2003;63:1351–8.
29. Amant F, Debiec-Rychter M, Schoenmakers EFPM, Hagemeijer-Hausman A, Vergote I. Cumulative dosage effect of a *RAD51L1/HMGA2* fusion and RAD51L1 loss in a case of pseudo-Meigs' syndrome. Genes Chromosomes Cancer 2001;32:324–9.
30. Blank C, Schoenmakers EFPM, Rogalla P, et al. Intragenic breakpoint within RAD51L1 in a t(6;14)(p21.3;q24) of a pulmonary chondroid hamartoma. Cytogenet Cell Genet 2001;95:17–9.
31. Nicodeme P, Geffroy S, Conti M, et al. Familial occurrence of thymoma and autoimmune diseases with the constitutional translocation t(14;20)(q24.1;p12.3). Genes Chromosomes Cancer 2005;44:154–60.
32. Miyagawa K, Tsuruga T, Kinomura A, et al. A role for *RAD54B* in homologous recombination in human cells. EMBO J 2002;21:175–80.
33. Tashiro S, Walter J, Shinohara A, Kamada N, Cremer T. Rad51 accumulation at sites of DNA damage and in postreplicative chromatin. J Cell Biol 2000;150:283–91.
34. Gough NM. Rapid and quantitative preparation of cytoplasmic RNA from small numbers of cells. Anal Biochem 1988;173:93–5.
35. Sonoda E, Sasaki MS, Morrison C, Yamaguchi-Iwai Y, Takata M, Takeda S. Sister chromatid exchanges are mediated by homologous recombination in vertebrate cells. Mol Cell Biol 1999;19:5166–9.
36. Bishop DK, Ear U, Bhattacharyya A, et al. Xrcc3 is required for assembly of Rad51 complexes *in vivo*. J Biol Chem 1998;273:21482–8.
37. Takata M, Sasaki MS, Tachiiri S, et al. Chromosome instability and defective recombinational repair in knockout mutants of the five Rad51 paralogs. Mol Cell Biol 2001;21:2858–66.
38. Yoshihara T, Ishida M, Kinomura A, et al. XRCC3 deficiency results in a defect in recombination and increased endoreduplication in human cells. EMBO J 2004;23:670–80.
39. Thompson LH, Schild D. Homologous recombinational repair of DNA ensures mammalian chromosome stability. Mutat Res 2001;477:131–53.
40. Deans B, Griffin CS, O'Regan P, Jasin M, Thacker J. Homologous recombination deficiency leads to profound genetic instability in cells derived from *Xrcc2*-knockout mice. Cancer Res 2003;63:8181–7.
41. Deans B, Griffin CS, Maconochie M, Thacker J. *Xrcc2* is required for genetic stability, embryonic neurogenesis, and viability in mice. EMBO J 2006;19:6675–85.
42. Masson J-Y, Tarsounas MC, Stasiak AZ, et al. Identification and purification of two distinct complexes containing the five RAD51 paralogs. Genes Dev 2001;15:3296–307.
43. Liu N, Schild D, Thelen MP, Thompson LH. Involvement of Rad51C in two distinct protein complexes of Rad51 paralogs in human cells. Nucleic Acids Res 2002;30:1009–15.
44. Daboussi F, Thacker J, Lopez BS. Genetic interactions between RAD51 and its paralogues for centrosome fragmentation and ploidy control, independently of the sensitivity to genetoxic stresses. Oncogene 2005;24:3691–86.
45. Hut HMJ, Lemstra W, Blaauw EH, van Cappellen GWA, Kampinga HH, Sibon OCM. Centrosome split in the presence of impaired DNA integrity during mitosis. Mol Biol Cell 2003;14:1993–2004.
46. Marx J. Debate surges over the origins of genomic defects in cancer. Science 2002;297:544–6.
47. Quintyne NJ, Reing JE, Hoffelder DR, Gollin SM, Saunders WS. Spindle multipolarity is prevented by centrosomal clustering. Science 2005;307:127–9.
48. Tarapore P, Fukasawa K. Loss of p53 and centrosome hyperamplification. Oncogene 2002;21:6234–40.
49. Sluder G, Nordberg JJ. The good, the bad, and the ugly: the practical consequences of centrosome amplification. Curr Opin Cell Biol 2004;16:49–54.

Published online February 2, 2006

880–892 Nucleic Acids Research, 2006, Vol. 34, No. 3
doi:10.1093/nar/gkj495

Haploinsufficiency of the Mus81–Eme1 endonuclease activates the intra-S-phase and G_2/M checkpoints and promotes rereplication in human cells

Takashi Hiyama[1,3], Mari Katsura[1], Takashi Yoshihara[1], Mari Ishida[1], Aiko Kinomura[1], Tetsuji Tonda[2], Toshimasa Asahara[3] and Kiyoshi Miyagawa[1,4,*]

[1]Department of Human Genetics and [2]Department of Environmetrics and Biometrics, Research Institute for Radiation Biology and Medicine and [3]Department of Surgery, Graduate School of Biomedical Sciences, Hiroshima University, 1-2-3 Kasumi, Minami-ku, Hiroshima 734-8553, Japan and [4]Section of Radiation Biology, Graduate School of Medicine, The University of Tokyo, 7-3-1 Hongo, Bunkyo-ku, Tokyo 113-0033, Japan

Received November 21, 2005; Revised and Accepted January 23, 2006

ABSTRACT

The Mus81–Eme1 complex is a structure-specific endonuclease that preferentially cleaves nicked Holliday junctions, 3′-flap structures and aberrant replication fork structures. *Mus81*$^{-/-}$ mice have been shown to exhibit spontaneous chromosomal aberrations and, in one of two models, a predisposition to cancers. The molecular mechanisms underlying its role in chromosome integrity, however, are largely unknown. To clarify the role of Mus81 in human cells, we deleted the gene in the human colon cancer cell line HCT116 by gene targeting. Here we demonstrate that Mus81 confers resistance to DNA crosslinking agents and slight resistance to other DNA-damaging agents. Mus81 deficiency spontaneously promotes chromosome damage such as breaks and activates the intra-S-phase checkpoint through the ATM-Chk1/Chk2 pathways. Furthermore, Mus81 deficiency activates the G_2/M checkpoint through the ATM-Chk2 pathway and promotes DNA rereplication. Increased rereplication is reversed by the ectopic expression of Cdk1. Haploinsufficiency of Mus81 or Eme1 also causes similar phenotypes. These findings suggest that a complex network of the checkpoint pathways that respond to DNA double-strand breaks may participate in some of the phenotypes associated with Mus81 or Eme1 deficiency.

INTRODUCTION

Precise replication of the entire genome during the S phase of the cell cycle is essential for cell survival. The progression of replication forks can be stalled in response to exogenous and endogenous sources, including depletion of deoxyribonucleotide pools, inhibition of replication proteins and aberrant DNA structures. Stalled replication forks can degenerate into broken forks, leading to chromosomal rearrangements and deletions (1). To avoid such deleterious events, all eukaryotes have evolved cell cycle checkpoint machinery and DNA repair pathways (2). The homologous recombination repair pathway contributes to the accurate repair of DNA damage; however, to promote cell survival, homologous recombination also participates in chromosomal rearrangements when replication forks are stalled (3).

Mus81 was originally identified as a member of the XPF family of endonucleases that physically interacts with Rad54 in *Saccharomyces cerevisiae* and Cds1 (Chk2) in *Schizosaccharomyces pombe* (4,5). The gene confers resistance to agents that lead to replication fork stalling or collapse, including ultraviolet (UV) radiation, methylmethane sulfonate (MMS), hydroxyurea and camptothecin, suggesting a role for Mus81 in the rescue of stalled and collapsed replication forks (6). In contrast, Mus81-deficient murine cells are not hypersensitive to camptothecin (7). The functional binding partner of the protein is MMS4 in *S.cerevisiae* (8) and Eme1 in *S.pombe* (9) and mammals (10–13). The synthetic lethality of *mus81* (or *mms4*) *sgs1* (or *top3*) double mutants suggests a functional link between Mus81 and Sgs1 helicases in the late steps of recombination (4,8). *In vitro*, the Mus81–Eme1 complex preferentially cleaves 3′-flap structures, various aberrant replication fork structures, and nicked Holliday junctions, suggesting that the complex plays a role in stalled replication fork processing and DNA repair by homologous recombination (14–16).

Loss of Mus81, MMS4 or Eme1 results in a reduction in sporulation and spore viability in yeast (8,9,17). Poor spore viability in *mus81* or *eme1* mutants of *S.pombe* is suppressed

*To whom correspondence should be addressed. Tel: +81 358413503; Fax: +81 358413013; Email: miyag-tky@umin.ac.jp

by eliminating Rec6 or Rec12, proteins required for the formation of double-strand breaks (DSBs), which initiates meiotic recombination. Expression of the bacterial Holliday junction resolvase RusA has been found to rescue the *mus81* meiotic defect (9). Thus, Mus81, MMS4 and Eme1 have been implicated in the processing of homologous recombination intermediates in yeast meiosis. The role of the Mus81–Eme1 complex in mitotic homologous recombination in mammals, however, remains uncertain (10,11,18). Remarkably, both *Mus81*$^{+/-}$ and *Mus81*$^{-/-}$ mice exhibit a profound predisposition to lymphomas and other cancers (18), although a subsequent study found no increased susceptibility to cancer in a different *Mus81*$^{-/-}$ model (7).

The role of Mus81 in genome integrity in response to replication stress has been proposed to be related to its physical association with Cds1 (Chk2) in fission yeast (19). Cds1-dependent phosphorylation of Mus81 prevents it from cleaving stalled replication forks that lead to replication fork breakage and chromosomal rearrangements by dissociating it from chromatin in cells exposed to hydroxyurea. Spontaneous and mitomycin C (MMC)-induced DNA damage such as breaks and triradial exchanges is increased in *Mus81*$^{+/-}$ and *Mus81*$^{-/-}$ mouse cells. In addition to these aberrations, the mutant cells have been shown to have an increased rate of aneuploidy (18).

Despite accumulating evidence that Mus81 plays a role in the processing of aberrant replication fork structures, the molecular mechanisms underlying its role in chromosome stability remain unclear. To clarify the role of Mus81–Eme1 in human cells, we deleted the genes in the human colon cancer cell line HCT116 by gene targeting. The advantages of using this cell line are that it allows efficient gene targeting in the presence of an intact p53 gene (20) and the cellular ploidy is stable. Here we show that Mus81 deficiency activates the intra-S-phase and G_2/M checkpoints and promotes DNA rereplication. This promotion of DNA rereplication was reversed by the forced expression of Cdk1. These findings provide new insight into the role of the Mus81–Eme1 complex in the control of human cell ploidy.

MATERIALS AND METHODS

Gene targeting at the Mus81 and Eme1 loci in HCT116

Targeting vectors were designed for in-frame insertion of promoterless drug resistance genes in exon 3 of *Mus81* or in exon 2 of *Eme1*. A 2.5 kb 5′-homology arm of *Mus81* was amplified by PCR from the isogenic DNA of HCT116 cells using primers 5′-GCCATGTCCAACGTCAGTA-3′ and 5′-ATCGATTCTCTCCAGATGGTGAGT-3′. A 1.7 kb 3′-homology arm of *Mus81* was amplified using primers 5′-ATCGATACTTGCGGAAGTCCA-3′ and 5′-AGGCAGAGGGGACAACACAG-3′. A 2.6 kb 5′-homology arm of *Eme1* was amplified using primers 5′-TTCACAGCACTTGCCAGTCT-3′ and 5′-ATCGATAATCCAGTGAGGGTGATGAC-3′. A 1.8 kb 3′-homology arm of *Eme1* was amplified using primers 5′-ATCGATTGTGAAGCCTCCTGTCCT-3′ and 5′-GGAACTGTCCTGTGTTACTG-3′. Both arms were cloned into pCR2.1 (Invitrogen) by the TA cloning method. The 3′-arms of *Mus81* and *Eme1* were excised by digestion with ClaI/SpeI and ClaI/XhoI, respectively, and subcloned into the vectors containing the 5′-arms. Neomycin and blasticidin resistance cassettes were inserted into the ClaI site of the vector containing both arms. Gene targeting in HCT116 was performed as described previously (21).

Ectopic expression of the Mus81 and Eme1 cDNAs

The human *Mus81* cDNA was amplified by PCR from cDNA derived from normal human cells using primers 5′-TGATCTCAACGGTCCTGC-3′ and 5′-GGGCTGTTTCACGGCATAA-3′. The human *Eme1* cDNA was amplified using primers 5′-AGTTGAAAGAGTGGCGGGA-3′ and 5′-CTCATCCCTGAGGGCTAGAA-3′. The cDNAs were inserted into pCR2.1, and the sequences were confirmed. The expression vectors were designed to insert the genes under the control of the MSV enhancer and the MMTV promoter. Transfected cells were selected in the presence of 900 μg/ml Zeocin™ (Invitrogen).

Sensitivity to DNA-damaging agents

Sensitivity to MMC was measured as described previously (22). To measure sensitivity to hydroxyurea, we plated the cells at a density of 2×10^3 cells per 60 mm dish, treated them with the agent for 6 h, and washed them three times with phosphate-buffered saline (PBS). To measure the sensitivity to UV treatment, we plated the cells at the same density and irradiated them. After 7 days of culturing, colonies were counted. Sensitivity to other DNA-damaging agents was measured as described previously (21). When knockout or complemented cells showed slow growth compared to wild-type cells, colonies were further cultured for 2 to 3 days and counted.

Focus formation of Rad51 and Rad54

Radiation-induced focus formation of Rad51 and Rad54 was performed as described previously (21). MMC-induced focus formation was examined by treatment with 0.8 μg/ml MMC for 1 h.

Cell cycle analysis

Cell synchronization by double-thymidine block was performed as described previously (23). Flow cytometry was performed with a FACSCalibur (Becton Dickinson) using the CellQuest software package.

Kinase assay

Immunoprecipitation was performed in the presence of phosphatase inhibitors (5 μM cantharidin, 5 nM microcystin LR and 25 μM bromotetramisole oxalate) essentially as described (22). Immunoprecipitates were washed three times in lysis buffer and three times in 25 mM HEPES (pH 7.4). The kinase reaction was performed at 30°C for 20 min in a total of 40 μl of reaction buffer [25 mM HEPES (pH 7.4), 15 mM $MgCl_2$, 80 mM EGTA, 1 mM DTT, 0.1 mM ATP and 3 μCi [γ-^{32}P]ATP]. Histone H1 (10 μg) was used as a substrate for the cyclin E, cyclin A and cyclin B kinase assays. Glutathione *S*-transferase (GST)-Cdc25C (200–256) was used as a substrate for the Chk2 kinase assay and was prepared as follows. The Cdc25C (200–256) fragment was amplified by PCR from cDNA derived from normal human cells using primers 5′-GAAAGATCAAGAAGCAAAGGTGAGC-3′ and 5′-TAAGCCCTTCCTGAGCTT-3′ and inserted into pGEX-5X-1

(Amersham Pharmacia). The plasmid was then used to transform *Escherichia coli* BL21, and expression of the fusion protein was induced by adjusting the culture to 1 mM Isopropyl-β-D-thiogalactopyranoside (IPTG). The fusion protein was purified using a glutathione–Sepharose 4B column (Amersham Pharmacia). The kinase reaction products were boiled in sample buffer and analyzed by SDS–PAGE.

Antibodies

Antibodies to Mus81 (N-20), cyclin A (C-19), cyclin E (C-19), cyclin B1 (GNS1), Cdc2 (Cdk1) (17), Cdk2 (D-12), Chk2 (A-12), Chk1 (G-4), ATR (N-19) and actin (C-2) were from Santa Cruz Biotechnology. Antibodies to phospho-Chk2 (Thr-68), phospho-Chk1 (Ser-317) and p21 (DCS60) were from Cell Signaling Technology. The antibody to ATM (NB100–104) was from Novus Biologicals.

Immunofluorescence

Cells were grown overnight on coverslips and fixed for 10 min in 4% paraformaldehyde. Cells were blocked with 10% horse serum and incubated with primary antibodies at room temperature for 1 h and with secondary antibodies for 30 min. Finally, cells were counterstained with 4′,6′-diamidino-2-phenylindole (DAPI) and mounted.

siRNA transfection

Eight hours prior to transfection, cells for the assay of ATM and ATR expression were seeded in a 100 mm dish at 1×10^6 cells/dish. Cells for immunofluorescence were seeded on coverslips at 1×10^5 cells/coverslip. The siRNA sequences for ATM used in the study were 5′-CAUCUAGAUCGGCAUUCAGtt-3′ and 5′-UGGUGCUAUUUAACGGAGCUtt-3′. The siRNA sequence for ATR was 5′-AACCUCCGUGAUGUUGCUUGAtt-3′. These siRNAs were synthesized by Sigma Genosys. A siCONTROL nontargeting siRNA from Dharmacon was used as a negative control. Transfection was performed using Lipofectamine 2000 transfection reagent (Invitrogen) according to the manufacturer's instructions. For western blot analysis, the Lipofectamine–siRNA complex was not removed during incubation. Cells were harvested at 48 h post-transfection. For immunofluorescence after double-thymidine block, the transfection mixture was removed after the first thymidine block.

Ectopic expression of Cdk1

The human *Cdk1* cDNA was amplified by PCR from cDNA derived from normal human cells using primers 5′-GCTCTTGGAAATTGAGCGGA-3′ and 5′-AGAAGACGAAGTACAGCTGAAGT-3′. The cDNAs were inserted into pCR2.1, and the sequences were confirmed. The *Cdk1* expression vector was designed to insert the gene under the control of the MSV enhancer and the MMTV promoter. Cdk1-overexpressing cells were selected in the presence of 900 μg/ml Zeocin™ (Invitrogen).

RESULTS

Generation of Mus81-deficient HCT116 cells

To investigate Mus81 function in human cells, we inactivated its gene in HCT116 cells by gene targeting. Targeting vectors were designed such that exon 3 was disrupted by promoterless antibiotic-resistance genes (Figure 1A). We obtained two independent $Mus81^{+/-}$ clones from 744 neomycin-resistant colonies and two $Mus81^{-/-}$ clones from 2380 neomycin- and blasticidin-resistant colonies derived from a single $Mus81^{+/-}$ clone (#653). Southern blot analysis using both 5′- and 3′-probes confirmed that both wild-type alleles had been correctly inactivated by gene targeting in the $Mus81^{-/-}$ cells (Figure 1B). Northern blot analysis revealed no expression of the gene in these clones (Figure 1C). Because no additional bands were detected using the full-length *Mus81* cDNA as a probe, it is unlikely that aberrant transcripts were generated by the disruption of exon 3. The correct targeting events were confirmed by western blot analysis (Figure 1D). Levels of expression comparable to or much higher than that of endogenous expression were achieved in these mutants by the introduction of the human *Mus81* cDNA.

Generation of Eme1-deficient HCT116 cells

To compare the role of Mus81 in human cells with that of Eme1, exon 2 of *Eme1* was disrupted by a neomycin resistance gene (Figure 1E). We obtained two independent $Eme1^{+/-}$ cells from 5250 neomycin-resistant colonies. $Eme1^{-/-}$ cells were not successfully generated because $Eme1^{-/-}$ cells grow slowly; however, $Eme1^{+/-}$ cells were sufficient for the purpose of comparing the roles of these proteins. Southern and northern blot analyses confirmed the disruption of one allele of the gene (Figure 1F and G). A level of expression comparable to that of endogenous expression was achieved by the expression of human *Eme1* cDNA in $Eme1^{+/-}$ cells.

Roles of the Mus81–Eme1 complex in the sensitivity to DNA damage

We next examined the sensitivity of Mus81 or Eme1 mutant cells to DNA damage by measuring their ability to form colonies following exposure to DNA-damaging agents. Because knockout cells and some complemented cells grew slowly, we took the growth rate into account in the counting of colonies (see Materials and Methods). Modest sensitivity to MMC was observed in $Mus81^{+/-}$ cells (1.5-fold) and $Mus81^{-/-}$ cells (4-fold) (Figure 2A). We noted a similar mild sensitivity to cisplatin in $Mus81^{-/-}$ cells. Mus81 deficiency resulted in a slight sensitivity to UV radiation, MMS, hydroxyurea and ionizing radiation (Figure 2B–G). The expression of *Mus81* cDNA in $Mus81^{-/-}$ cells restored the sensitivities to DNA-damaging agents to the wild-type levels. A slight increase in sensitivity to cisplatin, UV radiation and hydroxyurea was observed in $Mus81^{+/-}$ cells. A similar sensitivity to MMC and hydroxyurea was found in $Eme1^{+/-}$ cells. The expression of Eme1 only partially complemented the sensitivity to MMC. This is probably explained by the level of Eme1 expression in complemented cells: even if levels comparable to the endogenous levels are achieved by constitutive expression, they may not be sufficient for full complementation in response to DNA damage. Furthermore, the level of Mus81 expression is strictly dependent on the cell cycle (24), and the peak of Mus81 expression occurs in the S and G_2 phases. Like Mus81 expression, Eme1 expression may vary according to the stage of the cell cycle. These results indicate that Mus81 and Eme1 contribute to the resistance

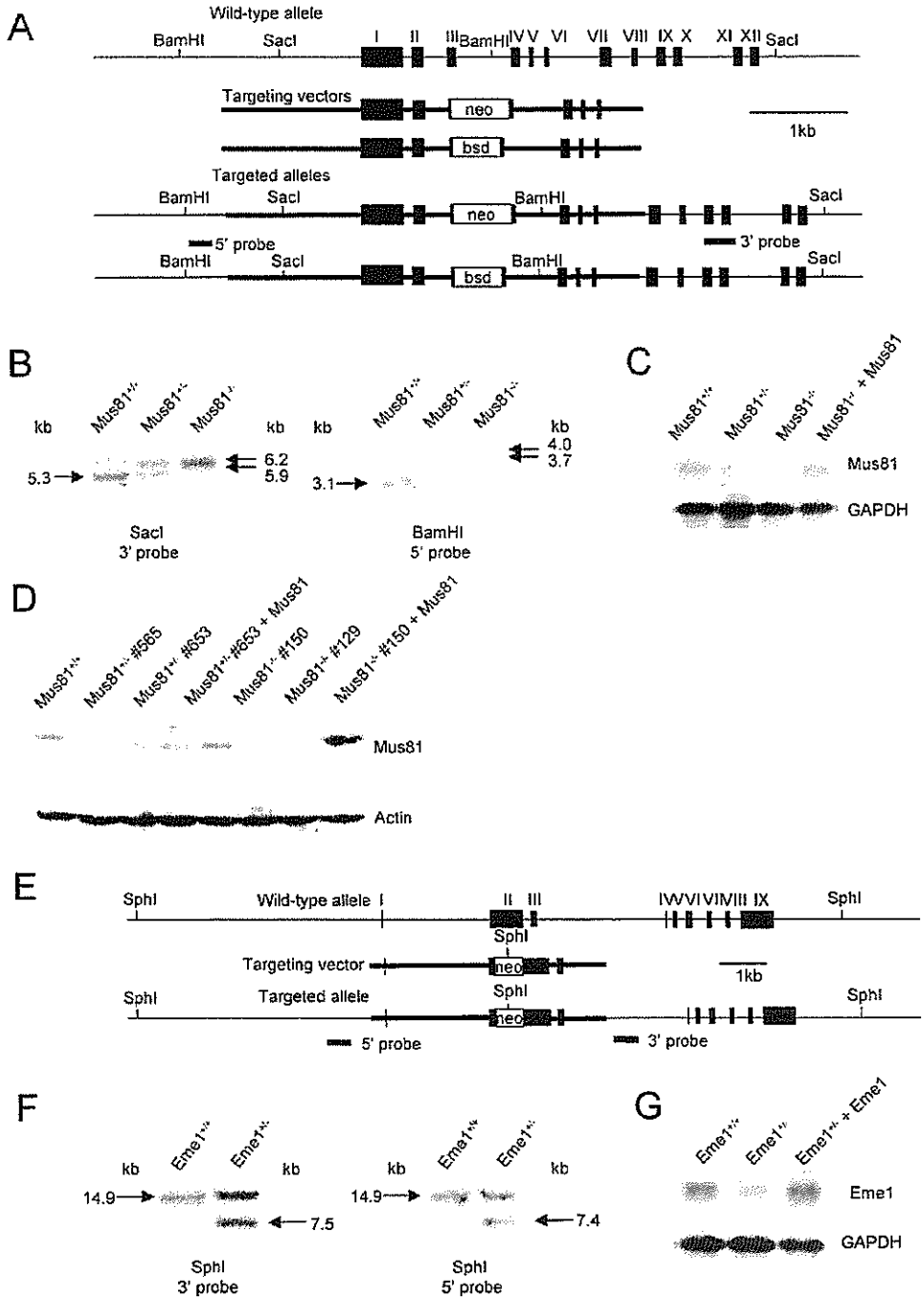

Figure 1. Generation of HCT116 cell lines deficient in Mus81 or Eme1 by gene targeting. (A) Schematic representation of the *Mus81* locus, the targeting vectors, and the targeted alleles. Relevant restriction sites and the position of the probes used for Southern blot analysis are shown. (B) Southern blot analysis confirming targeted integration at the *Mus81* locus. DNAs were digested with SacI or BamHI and hybridized with the probes depicted in (A). (C) Northern blot analysis confirming the expression levels of *Mus81*. Poly(A)$^+$ RNAs were isolated and hybridized with the full-length *Mus81* cDNA. Northern blotting for glyceraldehyde 3-phosphate dehydrogenase (GAPDH) was performed to confirm equal loading. (D) Western blot analysis confirming the protein expression levels of Mus81. Western blotting for actin was also carried out to confirm equal loading. (E) Schematic representation of the *Eme1* locus, the targeting vector and the targeted allele. Relevant restriction sites and the position of the probes used for Southern blot analysis are shown. (F) Southern blot analysis confirming targeted integration at the *Eme1* locus. DNAs were digested with SphI and hybridized with the probes depicted in (E). (G) Northern blot analysis confirming the expression levels of *Eme1*. Poly(A)$^+$ RNAs were isolated and hybridized with the full-length *Eme1* cDNA.

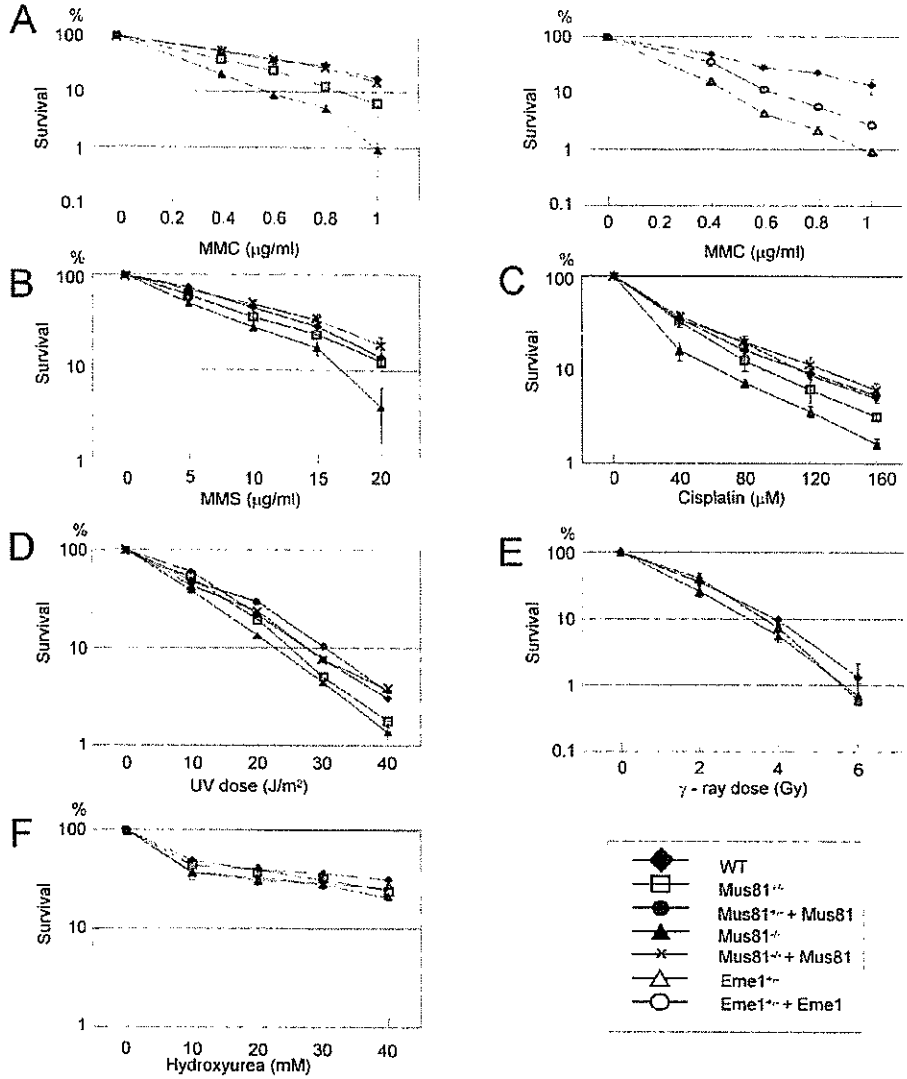

G

	MMC (μ g/ml)	MMS (μ g/ml)	Cisplatin (μ M)	UV (J/m^2)	IR (Gy)	HU (mM)
WT	0.62	12.50	28.64	13.63	1.68	23.70
$Mus81^{+/-}$	0.40	10.17	23.04	12.16	n.d.	22.02
$Mus81^{+/-}$ + Mus81	n.d.	n.d.	35.66	15.01	n.d.	n.d.
$Mus81^{-/-}$	0.16	7.91	5.68	7.64	1.02	9.70
$Mus81^{-/-}$ + Mus81	0.63	13.35	34.59	12.32	n.d.	n.d.
$Eme1^{+/-}$	0.08	n.d.	n.d.	n.d.	1.88	10.05
$Eme1^{+/-}$ + Eme1	0.37	n.d.	n.d.	n.d.	n.d.	n.d.

Figure 2. Sensitivity to DNA-damaging agents. (A–F) Sensitivities to MMC, MMS, cisplatin, UV radiation, ionizing radiation and hydroxyurea. Values represent the means ± the standard error of the mean for three independent experiments. *Mus81*$^{+/-}$ (#653), *Mus81*$^{-/-}$ (#150) and *Eme1*$^{+/-}$ (#376) cells were used. (G) D37 values of sensitivity to DNA-damaging agents. Graph Pad Prism4 software was used to calculate the values.

Figure 3. Chromosomal aberrations in *Mus81*$^{-/-}$ (#150) cells. The arrow in the left panel indicates a chromosome break. The arrow in the middle panel indicates a chromatid gap. Rereplication is shown in the right panel. In the left and middle panels, only a part of metaphase chromosome image is shown.

Table 1. Chromosomal aberrations

Cell line[a]	Chromatid-type[b] (%)	Chromosome-type[b] (%)	Abnormal cells[b] (excluding tetraploidy) (%)	Tetraploidy[c]
Mus81$^{+/+}$	2.5 ± 0.5	2.4 ± 1.1	4.5 ± 1.0	0.67% (23/3413)
Mus81$^{+/-}$	4.9 ± 1.2	6.2 ± 1.1	10.4 ± 1.1	1.88% (39/2077)
Mus81$^{+/-}$ + *Mus81*	3.2 ± 1.6	4.5 ± 1.5	6.7 ± 0.8	0.58% (6/1041)
Mus81$^{-/-}$	7.0 ± 1.3	10.0 ± 2.0	14.5 ± 0.5	2.46% (37/1503)
Mus81$^{-/-}$ + *Mus81*	2.4 ± 0.6	3.5 ± 1.5	5.7 ± 2.1	0.88% (27/3059)
Mus81$^{-/-}$ + *Cdk1*(#1)	6.2 ± 3.0	9.4 ± 4.1	12.9 ± 1.9	0.50% (10/2000)
Mus81$^{-/-}$ + *Cdk1*(#7)	4.0 ± 0.9	10.0 ± 0.5	11.2 ± 0.3	0.54% (6/1105)
Mus81$^{+/+}$ + *Cdk1*	2.5 ± 0.5	5.7 ± 1.6	6.9 ± 0.3	0.67% (2/300)
Eme1$^{+/-}$	6.4 ± 1.6	6.5 ± 1.3	10.7 ± 0.3	2.16% (63/2919)
Eme1$^{+/-}$ + *Eme1*	3.5 ± 0.9	5.2 ± 1.2	7.4 ± 1.3	1.20% (15/1248)

[a]*Mus81*$^{+/-}$ (#653), *Mus81*$^{-/-}$ (#150) and *Eme1*$^{+/-}$ (#376) cells were used.
[b]A total of 200 cells were scored for each line. Results represent the means ± SD of three independent experiments.
[c]The frequency of tetraploidy is shown as a percentage of tetraploid cells to the total number of metaphase cells analyzed; absolute numbers are given in parentheses.

of human cells to DNA-damaging agents such as DNA crosslinking agents.

Rad51 plays a central role in the early stages of homologous recombination and forms nuclear foci in a DNA damage-dependent manner (25). Impaired Rad51 focus formation has been reported in chicken and mammalian cells with defective homologous recombination (22,26,27). Rad54 plays a role in homologous recombination by dissociating Rad51 from nucleoprotein filaments formed on double-stranded DNA (28), and it forms nuclear foci that colocalize with foci of Rad51 (29). To investigate the role of Mus81 in the Rad51-dependent recombination pathway, we examined damage-dependent focus formation of Rad51 and Rad54 by treating cells with 0.8 μg/ml MMC or 8 Gy of ionizing radiation. We found no difference in focus formation between wild-type and *Mus81*$^{-/-}$ cells (data not shown), suggesting that Mus81 is not required for focus formation by these proteins.

Mus81–Eme1 is required for chromosome stability

A defect in homologous recombination repair leads to chromosome instability (30). We examined chromosomal aberrations in the presence of colcemid using metaphase spreads. The frequency of abnormal cells harboring chromatid- and chromosome-type aberrations such as gaps and breaks (Figure 3) was 4.5% in wild-type cells, whereas it increased to 10.4% in *Mus81*$^{+/-}$ cells and 14.5% in *Mus81*$^{-/-}$ cells (Table 1). Expression of the *Mus81* cDNA partially complemented these phenotypes (6.7 and 5.7%, respectively). The number of cells showing abnormalities was also increased in *Eme1*$^{+/-}$ cells (10.7%), and it was reduced by the expression of the *Eme1* cDNA (7.4%).

In addition to these aberrations, the numbers of tetraploid cells resulting from DNA rereplication (Figure 3) were significantly increased in the mutant cells (Table 1). The frequency of tetraploidy in wild-type cells was 0.67%, whereas it increased to 1.88% (*Mus81*$^{+/-}$) and 2.46% (*Mus81*$^{-/-}$) in the mutants. Differences in frequency were statistically significant between wild-type and *Mus81*$^{+/-}$ cells ($P < 1.0 \times 10^{-4}$) and *Mus81*$^{-/-}$ cells ($P < 1.0 \times 10^{-6}$). The differences were statistically evaluated using multiple logistic regression analysis taking Poisson errors into account. The expression of the *Mus81* cDNA in the mutants reduced the number of tetraploid cells to a level that was comparable to wild-type cells. The frequency of tetraploid cells was also increased to 2.16% in *Eme1*$^{+/-}$ cells ($P < 1.0 \times 10^{-5}$), and this value was reduced to 1.20% by the expression of the *Eme1* cDNA. Increases in DNA content resulting from DNA rereplication were not detected by FACS analysis, as only a small proportion of cells underwent rereplication.

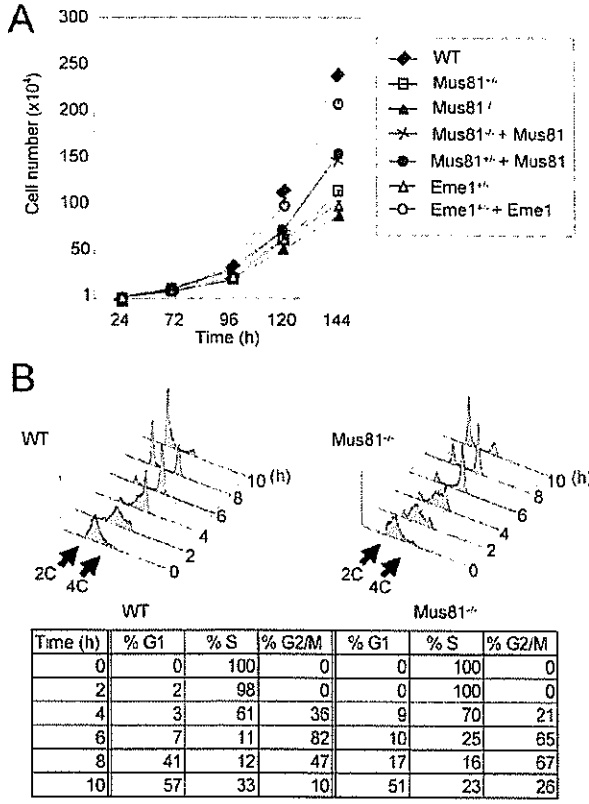

Time (h)	% G1	% S	% G2/M	% G1	% S	% G2/M
0	0	100	0	0	100	0
2	2	98	0	0	100	0
4	3	61	36	9	70	21
6	7	11	82	10	25	65
8	41	12	47	17	16	67
10	57	33	10	51	23	26

Figure 4. Effects of Mus81 or Eme1 deficiency on cell cycle progression. *Mus81*$^{+/-}$ (#653), *Mus81*$^{-/-}$ (#150) and *Eme1*$^{-/-}$ (#376) were examined. (**A**) Growth curves. The results show the means ± the standard error of the mean for three independent experiments. (**B**) Cell cycle distribution. The cells were synchronized in G_1/S by double-thymidine block and released. Samples were taken at the indicated time points and subjected to FACS analysis.

Mus81 or Eme1 deficiency affects cell cycle progression

The growth rates of *Mus81*$^{+/-}$, *Mus81*$^{-/-}$ and *Eme1*$^{-/-}$ cells were significantly lower than that of wild-type cells (Figure 4A). The doubling time of wild-type cells was 17 h, whereas the times for *Mus81*$^{+/-}$, *Mus81*$^{-/-}$ and *Eme1*$^{-/-}$ cells were 21, 22 and 21.5 h, respectively. Expression of the *Mus81* or *Eme1* cDNA partially complemented this phenotype. To examine the profiles of cell cycle progression, we performed FACS analysis using cells synchronized by double-thymidine block. We observed a small difference in the kinetics of accumulation of cells in the S and G_2/M phases between wild-type and *Mus81*$^{-/-}$ cells (Figure 4B). There was a peak in G_2/M phase accumulation 6 h after release in wild-type cells, whereas G_2/M phase accumulation was found 6 and 8 h after release in *Mus81*$^{-/-}$ cells.

Mus81 or Eme1 deficiency activates the intra-S-phase checkpoint

Cell cycle progression through S phase is regulated by cyclin E/Cdk2 and cyclin A/Cdk2. We therefore investigated the effects of Mus81 deficiency on the S phase progression by performing cyclin E and cyclin A kinase assays using lysates from cells synchronized in the G_1/S phase (Figure 5A). The cyclin E and cyclin A kinase activities were apparently lower in *Mus81*$^{-/-}$ cells than in wild-type cells at 0 and 0–8 h after release, respectively. Quantitative analysis revealed that *Mus81*$^{-/-}$ cells had a 40% reduction in cyclin E kinase activity at 0 h and a 50% reduction in cyclin A kinase activity at 4 h compared to wild-type cells. The levels of cyclin E and cyclin A in *Mus81*$^{-/-}$ cells were almost the same as in wild-type cells at this stage of the cell cycle, indicating that S phase checkpoint activation was responsible for the reductions in cyclin kinase activities.

Because the mutant cells showed a spontaneous delay of cell cycle progression during the S phase, we first investigated the effect of Mus81 deficiency on the ATR-Chk1 pathway, which regulates the basal turnover of Cdc25A (31). Western blot analysis using an anti-phospho-Chk1 antibody (Ser-317) revealed that levels of phospho-Chk1 were high in the early S phase and that the levels in *Mus81*$^{-/-}$ cells were the same as in wild-type cells (Figure 5B). This finding is consistent with the proposed role of Chk1 activation in the maintenance of the physiological turnover of Cdc25A.

However, the involvement of Chk1 in a DNA damage-dependent checkpoint cannot be evaluated by this method because the basal levels of phospho-Chk1 were high during the S phase. We therefore examined the damage-dependent Chk1 activation at the single-cell level by immunofluorescence using the same antibody (Figure 5C). Clear staining in the nucleus indicating the damage-dependent phosphorylation of Chk1 on Ser-317 was observed in a small proportion of cells. This staining pattern was found in 0.3 ± 0.1% (mean ± SD) of wild-type cells and in 1.9 ± 0.1% of *Mus81*$^{-/-}$ cells (n = 500). The frequencies of the staining ranged from 0.9 ± 0.1% to 1.5 ± 0.2% in *Mus81*$^{+/-}$ and *Eme1*$^{+/-}$ cells.

To investigate whether ATM or ATR regulates Chk1 activation by phosphorylation in the S phase, ATM and ATR were knocked down by siRNA (Figure 5D). Silencing of ATM reduced the frequency to 0.5 ± 0.3% in *Mus81*$^{-/-}$ cells, whereas silencing of ATR or transfection of control siRNA did not affect the frequency, indicating that the ATM-Chk1 pathway was activated in the S phase in *Mus81*$^{-/-}$ cells (Figure 5C). This pathway has been shown to be activated in response to DSBs induced by ionizing radiation (32).

The intra-S-phase checkpoint in response to DSBs was first shown to be mediated by the ATM-Chk2-Cdc25A-Cdk2 pathway (33). Next, we investigated Chk2 activation in the S phase by immunofluorescence using an anti-phospho-Chk2 (Thr-68) antibody (Figure 5E). Phosphorylation of Chk2 on Thr-68 is required for the initiation of Chk2 activity. Clear staining of phospho-Chk2 in the nucleus was not observed in wild-type cells, but it was observed in 2.3 ± 0.3% of *Mus81*$^{-/-}$ cells (n = 500). The frequency of the staining ranged from 1.0 ± 0.2% to 1.6 ± 0.2% in *Mus81*$^{+/-}$ and *Eme1*$^{+/-}$ cells, respectively. Silencing of ATM reduced the frequency to 0.7 ± 0.5%, whereas silencing of ATR or transfection of control siRNA did not affect the frequency, indicating that ATM acted as an upstream kinase for Chk2 activation. Thus, both the ATM-Chk1 and ATM-Chk2 checkpoint pathways were activated during the S phase in the Mus81 and Eme1 mutant cells.

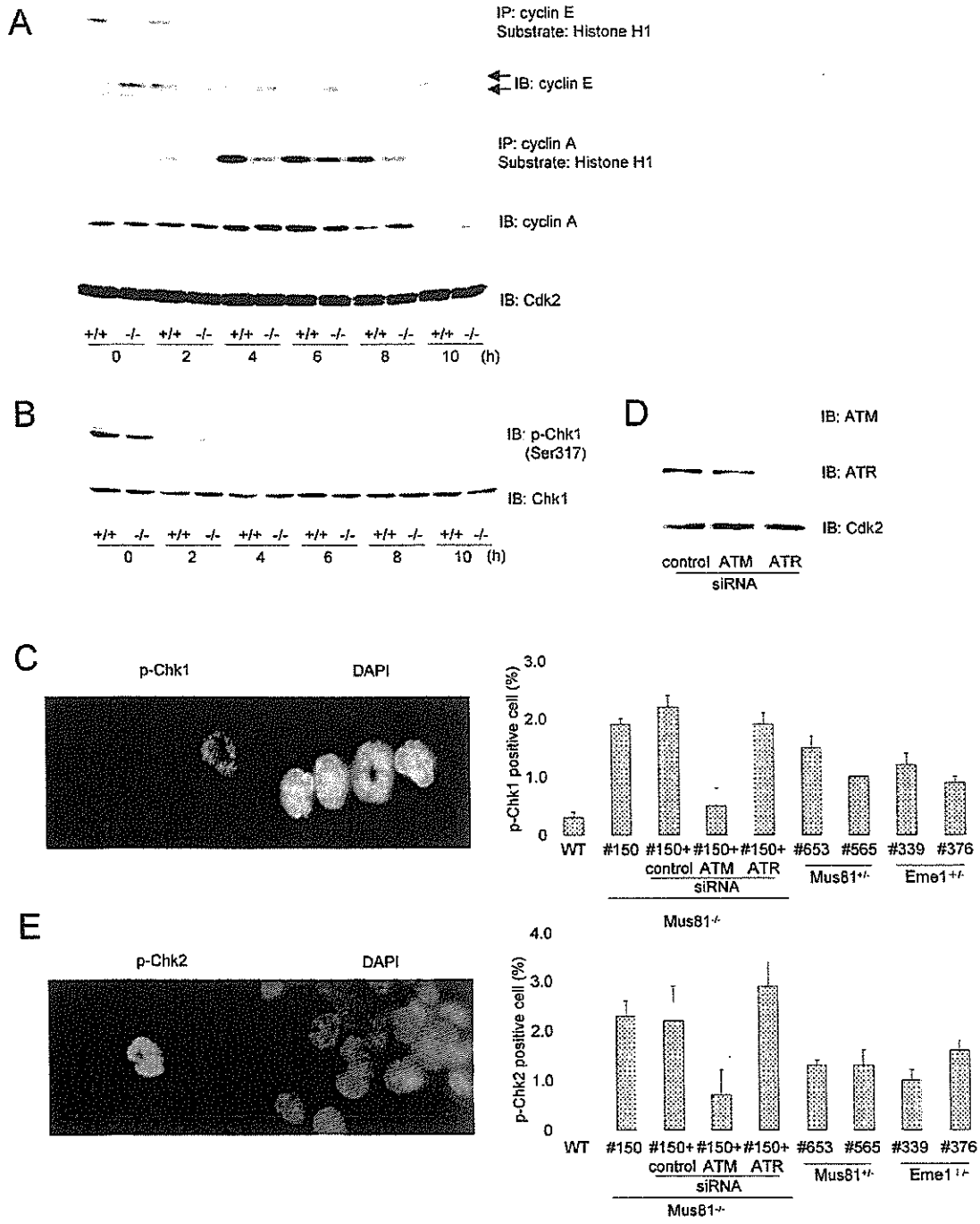

Figure 5. Activation of the intra-S-phase checkpoint. (A) Cyclin E and cyclin A kinase activities with histone H1 as the substrate. Wild-type and *Mus81*$^{-/-}$ (#150) cells were synchronized in G_1/S by double-thymidine block and released. (B) Western blot analysis of synchronized wild-type and *Mus81*$^{-/-}$ (#150) cell extracts using anti-phospho-Chk1 (Ser-317). The experiments in (A) and (B) were performed three times, and representative results are shown. (C) Immunofluorescence of *Mus81*$^{-/-}$ cells synchronized in S phase using anti-phospho-Chk1 (Ser-317). The frequencies of positive staining for phospho-Chk1 are shown in the right panel. (D) Western blot analysis of unsynchronized *Mus81*$^{-/-}$ (#150) cells transfected with siRNAs. The experiment was performed three times. (E) Immunofluorescence of *Mus81*$^{-/-}$ cells synchronized in S phase using anti-phospho-Chk2 (Thr-68). The frequencies of the positive staining of phospho-Chk2 are shown in the right panel. In (C) and (E), cells were fixed 2 h after release, and a total of 500 cells were examined for each cell line. The results represent the means ± standard deviation of three independent experiments. IB, immunoblot; IP, immunoprecipitation; p-Chk, phospho-Chk; WT, wild-type.

Mus81 or Eme1 deficiency activates the G_2/M checkpoint

Because FACS profiles revealed a difference in the accumulation of cells in G_2/M, we investigated the effects of Mus81 deficiency on the G_2/M delay by running a cyclin B kinase assay using cells synchronized in the G_1/S phase (Figure 6A). Cyclin B kinase activity was increased 6 h after release in wild-type cells, whereas an increase in the kinase activity was not obvious at 6 h but was clear at 8 h after release in the mutant. Repeated experiments demonstrated that such a difference between the wild-type and mutant cells could be observed either 6 or 8 h after release, consistent with the results from the FACS analysis. There were no apparent differences in cyclin B and Cdk1 levels between wild-type and *Mus81*$^{-/-}$ cells, excluding the possibility that reduced cyclin B kinase activity was due to repression of these proteins. In addition, we noticed that the level of cyclin B expression was high even in the G_1 phase at 10 h in the HCT116 cell line. This aberrant expression of cyclin B has been observed in some human cancer cells, suggesting that it may be associated with abnormal proliferation of cancer cells (34). The high level of cyclin B may account for the sustained cyclin B kinase activity during the early G_1 phase in wild-type cells.

Activation of Cdk1 by association with cyclin B is essential for the initiation of the M phase. The delay of cyclin B activity in *Mus81*$^{-/-}$ cells may simply indicate that the cell cycle progression was delayed by the preceding S phase delay. Alternatively, G_2/M checkpoint activation may be involved in the delay of cyclin B activity. Chk1 and Chk2 play a role in the G_2/M checkpoint as effector kinases (35). To investigate whether the G_2/M checkpoint was activated in the mutants, we therefore examined Chk1 and Chk2 kinase activities using a recombinant GST-Cdc25C (200–256) fusion protein as a substrate. These kinases preferentially phosphorylate Cdc25C on Ser-216 (36). We examined the difference in Chk2 kinase activity in synchronized cells. Chk2 kinase activity was significantly increased in the Mus81 mutant 6 h after release, whereas an increase was not evident in wild-type cells (Figure 6B). There were no differences in the levels of Chk2. A more than 3-fold increase in Chk2 activity was also observed in two *Mus81*$^{+/-}$ cell lines as well as in two *Eme1*$^{+/-}$ cell lines, excluding the possibility that activation of Chk2 was due to a clonal variation (Figure 6C). Expression of *Mus81* or *Eme1* cDNA reduced this increase in Chk2 activity in the mutant cells (Figure 6C). Chk2 kinase phosphorylation of Cdc25C was not clearly observed before 6 h, indicating that the increase in this activity at 6 h reflected the G_2/M checkpoint activation rather than a delay of the cell cycle progression. The S phase checkpoint was activated in *Mus81*$^{-/-}$ cells from 0 to 4 h after release.

The increase in Chk2 kinase activity was abolished in the presence of 0.5 mM caffeine (Figure 6C). Treatment with 0.5 mM caffeine for 1 h has little effect on DNA synthesis (37), excluding the possibility that the elimination of Chk2 activity by caffeine was due to the delay in cell cycle progression. Because caffeine inhibits ATM and ATR kinase activities (38–40), they are likely required for this increase in Chk2 kinase activity. For this reason, we further investigated the effect of siRNA silencing of ATM and ATR on Chk2 activity (Figures 5D and 6D). Chk2 activity was reduced by silencing of ATM but not by silencing of ATR, indicating that the activation of ATM in response to DNA damage is responsible for the increase in Chk2 activity in *Mus81*$^{-/-}$ cells. In contrast, there was no clear difference in the phosphorylation of GST-Cdc25C (200–256) by Chk1 in wild-type and *Mus81*$^{-/-}$ cells (Figure 6E). There was also no difference in p21 expression in wild-type and *Mus81*$^{-/-}$ cells (Figure 6F).

It is assumed that the p21-dependent G_2/M checkpoint leads to sustained cell cycle arrest, whereas the Cdc25-dependent checkpoint leads to transient delay (41). Consistent with this idea, many delayed cells eventually proceeded into the M and G_1 phases. These results show that, in addition to the intra-S-phase checkpoint, the G_2/M checkpoint was activated in the Mus81 mutant cells via the ATM-Chk2 pathway.

Overexpression of Cdk1 prevents rereplication

Because deletion of Cdk1 promotes DNA rereplication in human cells (42), reduced cyclin B kinase activity is likely to cause increased rereplication in Mus81 mutants. We examined this possibility by overexpressing Cdk1 in the Mus81 mutants. Cdk1 kinase activity is regulated by accumulation of Cdk1-associated cyclin B and removal of inhibitory protein phosphorylations. Western blot analysis revealed that levels of cyclin B were high in G_2/M in *Mus81*$^{-/-}$ cells while the levels of Cdk1 were constant, suggesting that overexpressed Cdk1 may be associated with endogenous cyclin B. Given that overexpressed Cdk1 is not phosphorylated on inhibitory phosphorylation sites by overcoming Wee1 and Myt1 kinase activities, Cdk1 activity is expected to be increased. Because we showed that p21 is not induced in *Mus81*$^{-/-}$, it is not necessary to consider direct inhibition of Cdk2 activity by p21. Consistent with this hypothesis, the reduction of cyclin B kinase activity was reversed by the overexpression of Cdk1 (Figure 6G). The increase in cyclin B activity by ectopic expression of Cdk1 reduced the frequency of tetraploidy from 2.46 to 0.50% and 0.54% in the two *Mus81*$^{-/-}$ cell lines ($P < 1.0 \times 10^{-2}$) (Table 1). Thus, the increased rereplication in Mus81 mutants was reversed by ectopic expression of Cdk1.

DISCUSSION

In the current studies, we demonstrated that Mus81–Eme1 deficiency activates the intra-S-phase and G_2/M checkpoints in response to DNA damage and promotes DNA rereplication. In addition, we confirmed that the Mus81–Eme1 complex contributes to the resistance against DNA-damaging agents in human cells. These assays show quite small differences, suggesting that there may be functional redundancy between the Mus81–Eme1 complex and other repair proteins in the response to DNA damage. Consistent with extensive genetic studies in yeast, the results of the present study indicate that there is no functional difference between Mus81 and Eme1 in human cells.

Identification of the physiological substrates of the Mus81–Eme1 complex has long remained elusive. However, a study showing the presence of resolvase activities in two separate fractions from human cell extracts has significantly enhanced our understanding of this complex system (43,44). The Mus81–Eme1 complex shows a greater activity for the

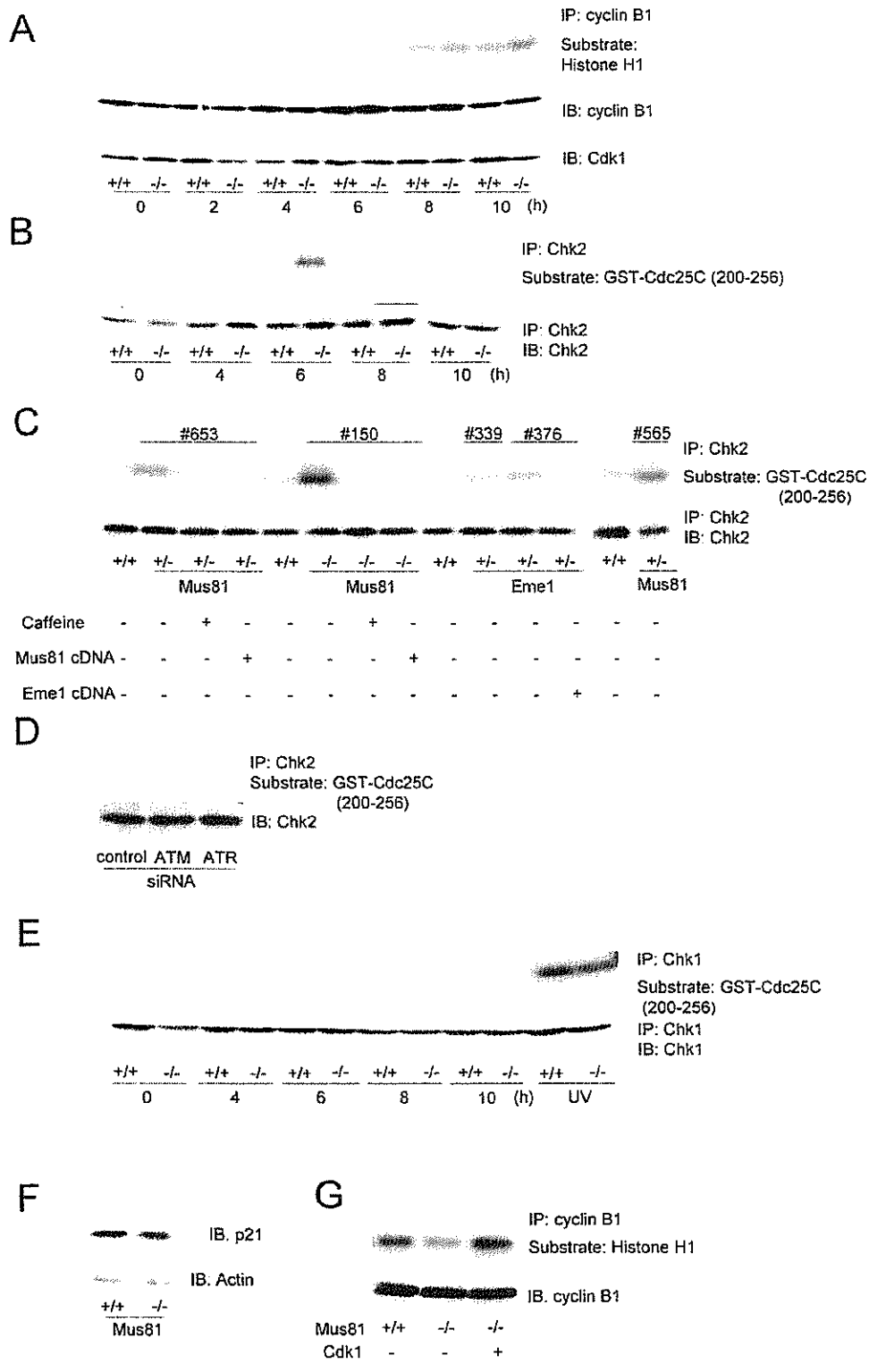
A
IP: cyclin B1
Substrate:
Histone H1
IB: cyclin B1
IB: Cdk1
+/+ -/- +/+ -/- +/+ -/- +/+ -/- +/+ -/- +/+ -/-
0 2 4 6 8 10 (h)
B
IP: Chk2
Substrate: GST-Cdc25C (200-256)
IP: Chk2
IB: Chk2
+/+ -/- +/+ -/- +/+ -/- +/+ -/- +/+ -/-
0 4 6 8 10 (h)
C
#653 #150 #339 #376 #565
IP: Chk2
Substrate: GST-Cdc25C
(200-256)
IP: Chk2
IB: Chk2
+/+ +/- +/- +/- +/+ -/- -/- -/- +/+ +/- +/- +/- +/+ +/-
Mus81 Mus81 Eme1 Mus81
Caffeine - - + - - - + - - - - - - -
Mus81 cDNA - - - + - - - + - - - - - -
Eme1 cDNA - - - - - - - - - - - + - -
D
IP: Chk2
Substrate: GST-Cdc25C
(200-256)
IB: Chk2
control ATM ATR
siRNA
E
IP: Chk1
Substrate: GST-Cdc25C
(200-256)
IP: Chk1
IB: Chk1
+/+ -/- +/+ -/- +/+ -/- +/+ -/- +/+ -/- +/+ -/-
0 4 6 8 10 (h) UV
F
IB. p21
IB. Actin
+/+ -/-
Mus81
G
IP: cyclin B1
Substrate: Histone H1
IB. cyclin B1
Mus81 +/+ -/- -/-
Cdk1 - - +

3′-flap and three-way branched fork structures, whereas the Rad51C complex shows specific activity for Holliday junctions. These findings suggest that replication forks or 3′-flaps may be the *in vivo* substrates of the Mus81 endonuclease. The present finding that the Mus81–Eme1 complex confers resistance to DNA crosslinking agents, MMS and hydroxyurea supports this idea because these agents cause stalled replication forks. However, it is also possible that recombination intermediates such as D-loops and Holliday junctions are the *in vivo* substrates of the endonuclease. This possibility is supported by the observation that mutations in genes such as *RAD51*, *RAD52*, *RAD55* and *RAD57* that play early roles in recombination suppress the synthetic lethality of *mus81* (or *mms4*) *sgs1* (or *top3*) mutants (45,46). If Mus81-Mms4 directly cleaves replication forks and does not play a late role, synthetic lethality would not be rescued by a defect in these genes. The physical interaction of Mus81 with Rad54 in yeast is consistent with this idea (5). Furthermore, Mus81 has been shown to play a key role in the Rhp51-independent recombination repair pathway in fission yeast by resolving D-loops formed by Rad22 (47).

We observed spontaneous activation of the intra-S-phase checkpoint through two independent cascades in *Mus81*$^{-/-}$ cells. The ATM-Chk2-Cdc25A-Cdk2 pathway has been shown to play a role in the intra-S-phase checkpoint in response to DSBs. In addition, the damage-dependent Chk1 pathway was activated by ATM but not by ATR. This finding strongly suggests that the Mus81–Eme1 complex is involved in the processing of DSBs. This notion is also supported by the present finding that Mus81 or Eme1 deficiency led to the activation of the G_2/M checkpoint through the ATM-Chk2 pathway. DSBs that escape the intra-S-phase checkpoint and/or DSBs generated in G_2 can activate the G_2/M checkpoint. Thus, the recombination intermediates are likely to be the *in vivo* target of the Mus81–Eme1 complex. It is also possible that stalled replication forks, if unprocessed, generate DSBs, which could activate the ATM-dependent checkpoint pathway. In contrast to ATM, ATR kinase activity is activated by several kinds of DNA damage, including those caused by UV radiation and chemicals that make bulky base lesions, as well as by stalled replication forks (48). Although the present study demonstrated that Chk1 is not activated by ATR, it is very likely that ATR was activated in *Mus81*$^{-/-}$ cells. Despite the fact that cyclin A activity was strongly repressed, activation of Chk1 and Chk2 could account for the S phase delay only in a small proportion of the Mus81 and Eme1 mutant cells. In addition to the intra-S-phase checkpoint, the replication checkpoint initiated by ATR is likely to play a major role in the S phase delay resulting from Mus81 or Eme1 deficiency. Identification of the effectors that protect the replication fork will address this issue.

Mus81 has been shown to be physically associated with Cds1 (Chk2) in yeast and in human cells, suggesting a functional link between these proteins. We found that ionizing radiation- or MMC-induced phosphorylation of Chk2 on Thr-68 is not affected by a deficiency of Mus81 (data not shown), suggesting that Mus81 does not directly regulate the function of Chk2. Conversely, phosphorylation of Mus81 by Chk2 has been shown to be required for the maintenance of genome integrity during replication stress (19).

Evidence for the molecular mechanisms underlying checkpoint activation in response to DNA damage has largely come from studies in cells exposed to DNA-damaging agents. In contrast to these studies, our results provide new insight into the mechanism of checkpoint activation in response to DNA damage that spontaneously arises from a defect in a single process of DNA repair where there is no exogenous DNA damage. Reactive cellular metabolites are assumed to become endogenous genotoxic insults. Because the cells were more sensitive to DNA crosslinking agents than other agents, it is of interest to identify the sources of endogenous DNA interstrand crosslinks.

In addition to increased chromosomal aberrations such as gaps and breaks, we found increased frequencies of tetraploidy in the Mus81–Eme1 mutants. In yeast, B-type cyclin-dependent kinases prevent rereplication by several overlapping mechanisms, including phosphorylation of ORC, down-regulation of Cdc6 and nuclear exclusion of MCM proteins (49). The ability of these kinases to prevent rereplication is also supported by the finding that cyclin B/Cdk1 is associated with replication origins (50). In human cells, deletion of Cdk1 by gene targeting results in increased levels of tetraploidy (42). It is therefore likely that reduced cyclin B/Cdk1 kinase activity caused increased rereplication in the Mus81 mutants. This model is supported by our finding that the overexpression of Cdk1 prevents rereplication in Mus81 mutants, although we cannot exclude the possibility that Cdk1 overexpression plays an indirect role in preventing rereplication. Chromosomes in tetraploid cells are very unstable, as demonstrated by the finding that tetraploid-derived mouse tumors have numerical and structural chromosomal aberrations (51). The aneuploidy observed in mouse *Mus81*$^{-/-}$ cells may result from chromosome instability in tetraploid cells. Recent evidence has suggested that aneuploid cells proceed through a tetraploid state (52). This possibility may also account for the absence of a clear peak of 8C DNA content in *Mus81*$^{-/-}$ cells in FACS profiles. We observed extremely low frequency of DNA contents ranging from 4C to 8C at high magnification, which apparently concealed a small peak at 8C.

Haploinsufficiency of *Mus81* was found to cause phenotypes similar to those of a complete loss of the gene. Similar results were observed for *Mus81*$^{+/-}$ and *Mus81*$^{-/-}$ mice. Loss

Figure 6. Activation of the G_2/M checkpoint. (**A**) Cyclin B kinase activity with histone H1 as the substrate. Wild-type and *Mus81*$^{-/-}$ (#150) cells were synchronized in G_1/S by double-thymidine block and released. (**B**) Chk2 kinase activity using GST-Cdc25C (200–256) as the substrate and whole-cell extracts from wild-type and *Mus81*$^{-/-}$ (#150) cells synchronized in G_1/S and released. The experiments in (**A**) and (**B**) were performed five times. (**C**) Chk2 kinase activity on GST-Cdc25C (200–256) of synchronized cells harvested 6 h after release. For caffeine treatment, cells were incubated in the presence of 0.5 mM caffeine for 1 h prior to cell lysis. (**D**) The effects of ATM and ATR on Chk2 activity. Shown is the Chk2 kinase activity using GST-Cdc25C (200–256) as a substrate in extracts of *Mus81*$^{-/-}$ (#150) cells harvested 48 h after transfection with siRNA. (**E**) Chk1 kinase activity using GST-Cdc25C (200–256) as a substrate in extracts from wild-type and *Mus81*$^{-/-}$ (#150) cells synchronized in G_1/S and released. Cells treated with UV radiation are used as positive controls. The treated cells were harvested 5 h after UV radiation (40 J/m^2). The experiments in (**C**), (**D**) and (**E**) were performed twice, and representative results are shown. (**F**) Western blot analysis of extracts from unsynchronized cells using an anti-p21 antibody. (**G**) Cyclin B kinase activity with histone H1 as a substrate in extracts from unsynchronized cells. In (**F**) and (**G**), *Mus81*$^{-/-}$ (#150) cells were used.

of heterozygosity is commonly observed in tumors. The human *Mus81* gene maps to chromosome 11q13.1. Although loss of heterozygosity at the *Mus81* locus in tumors has not been reported, normal or precancerous cells have a chance to lose one allele of *Mus81*. Given that cells lose one copy of *Mus81* during tumor progression, aberrant replication fork structures and recombination intermediates are expected to accumulate and eventually lead to further genomic instability. Haploinsufficiency of *Mus81* may contribute to tumor progression through this mechanism. It is noteworthy that predisposition to cancer was not observed over 15 months in another *Mus81*$^{-/-}$ mouse model (7). This discrepancy may be explained by a difference in strains. However, it is most likely that Mus81 deficiency does not directly contribute to tumor formation but rather induces chromosome aberrations such as aneuploidy that do not directly lead to cancer. A long latency, during which chromosomal aberrations accumulate, may be required for tumor formation in such a situation. It is also possible that additional modifiers that promote different types of genomic instability are required for tumor formation.

The present finding that small changes in the gene dosage of Mus81–Eme1 promote rereplication implicates the significance of small amounts of genotoxic insults in chromosome stability. Even in the absence of exogenous genotoxic sources, endogenous insults can lead to chromosome instability by damaging DNA. Aberrant fork structures and recombination intermediates are expected to accumulate in cells exposed to genotoxic insults. These cells suffer from increased rereplication in response to DNA damage, which does not immediately lead to tumor-associated genomic aberrations. Instead, this pathway can contribute to tumor development by inducing centrosome dysfunction and aneuploidy after numerous rounds of the cell cycle. This scenario may explain cases of radiation-induced carcinogenesis in which patients develop tumors after long periods of exposure to low-dose radiation.

ACKNOWLEDGEMENTS

The authors would like to thank M. Ohtaki for statistical analyses. The authors also thank A. Shinohara for providing the anti-Rad51 and anti-Rad54 antibodies. This work was supported by the Ministry of Education, Culture, Sports, Science and Technology and by the Ministry of Health, Labor and Welfare of Japan. M.K. and T.Y. were supported by the Hiroshima University 21st Century COE Program. Funding to pay the Open Access publication charges for this article was provided by the Ministry of Education, Culture, Sports, Science and Technology of Japan.

Conflict of interest statement. None declared.

REFERENCES

1. Branzei,D. and Foiani,M. (2005) The DNA damage response during DNA replication. *Curr. Opin. Cell Biol.*, **17**, 568–575.
2. Sancar,A., Lindsey-Boltz,L.A., Unsal-Kacmaz,K. and Linn,S. (2004) Molecular mechanisms of mammalian DNA repair and the DNA damage checkpoints. *Annu. Rev. Biochem.*, **73**, 39–85.
3. Lambert,S., Watson,A., Sheedy,D.M., Martin,B. and Carr,A.M. (2005) Gross chromosomal rearrangements and elevated recombination at an inducible site-specific replication fork barrier. *Cell*, **121**, 689–702.
4. Boddy,M.N., Lopez-Girona,A., Shanahan,P., Interthal,H., Heyer,W.-D. and Russell,P. (2000) Damage tolerance protein Mus81 associates with the FHA1 domain of checkpoint kinase Cds1. *Mol. Cell. Biol.*, **20**, 8758–8766.
5. Interthal,H. and Heyer,H.-D. (2000) *MUS81* encodes a novel Helix-hairpin-Helix protein involved in the response to UV- and methylation-induced DNA damage in *Saccharomyces cerevisiae*. *Mol. Gen. Genet.*, **263**, 812–827.
6. Doe,C.L., Ahn,J.S., Dixon,J. and Whitby,M.C. (2002) Mus81-Eme1 and Rqh1 involvement in processing stalled and collapsed replication forks. *J. Biol. Chem.*, **277**, 32753–32759.
7. Dendouga,N., Gao,H., Moechars,D., Janicot,M., Vialard,J. and McGowan,C.H. (2005) Disruption of murine Mus81 increases genomic instability and DNA damage sensitivity but does not promote tumorigenesis. *Mol. Cell. Biol.*, **25**, 7569–7579.
8. Kaliraman,V., Mullen,J.R., Fricke,W.M., Bastin-Shanower,S.A. and Brill,S.J. (2001) Functional overlap between Sgs1-Top3 and the Mms4-Mus81 endonuclease. *Genes Dev.*, **15**, 2730–2740.
9. Boddy,M.N., Gaillard,P.-H.L., McDonald,W.H., Shanahan,P., Yates,J.R.,III and Russell,P. (2001) Mus81-Eme1 are essential components of a Holliday junction resolvase. *Cell*, **107**, 537–548.
10. Abraham,J., Lemmers,B., Hande,M.P., Moynahan,M.E., Chahwan,C., Ciccia,A., Essers,J., Hanada,K., Chahwan,R., Khaw,A.K. *et al.* (2003) Eme1 is involved in DNA damage processing and maintenance of genomic stability in mammalian cells. *EMBO J.*, **22**, 6137–6147.
11. Blais,V., Gao,H., Elwell,C.A., Boddy,M.N., Gaillard,P.-H.L., Russell,P. and McGowan,C.H. (2004) RNA interference inhibition of Mus81 reduces mitotic recombination in human cells. *Mol. Biol. Cell*, **15**, 552–562.
12. Ciccia,A., Constantinou,A. and West,S.C. (2003) Identification and characterization of the human Mus81-Eme1 endonuclease. *J. Biol. Chem.*, **278**, 25172–25178.
13. Ogrunc,M. and Sancar,A. (2003) Identification and characterization of human MUS81-MMS4 structure specific endonuclease. *J. Biol. Chem.*, **278**, 21715–21720.
14. Chen,X.-B., Melchionna,R., Denis,C.-M., Gaillard,P.-H.L., Blasina,A., Van de Weyer,I., Boddy,M.N., Russell,P., Vialard,J. and McGowan,C.H. (2001) Human Mus81-associated endonuclease cleaves Holliday junctions *in vitro*. *Mol. Cell*, **8**, 1117–1127.
15. Gaillard,P.-H.L., Noguchi,E., Shanahan,P. and Russell,P. (2003) The endogenous Mus81–Eme1 complex resolves Holliday junctions by a nick and counternick mechanism. *Mol. Cell*, **12**, 747–759.
16. Osman,F., Dixon,J., Doe,C.L. and Whitby,M.C. (2003) Generating crossovers by resolution of nicked Holliday junctions: a role for Mus81-Eme1 in meiosis. *Mol. Cell*, **12**, 761–774.
17. de los Santos,T., Loidl,J., Larkin,B. and Hollingsworth,N.M. (2001) A role for *MMS4* in the processing of recombination intermediates during meiosis in *Saccharomyces cerevisiae*. *Genetics*, **159**, 1511–1525.
18. McPherson,J.P., Lemmers,B., Chahwan,R., Pamidi,A., Migon,E., Matysiak-Zablock,E., Moynahan,M.E., Essers,J., Hanada,K., Poonepalli,A. *et al.* (2004) Involvement of mammalian Mus81 in genome integrity and tumor suppression. *Science*, **304**, 1822–1826.
19. Kai,M., Boddy,M.N., Russell,P. and Wang,T.S.-F. (2005) Replication checkpoint kinase Cds1 regulates Mus81 to preserve genome integrity during replication stress. *Genes Dev.*, **19**, 919–932.
20. Michel,L.S., Liberal,V., Chatterjee,A., Kirchwegger,R., Pasche,B., Gerald,W., Dobles,M., Sorger,P.K., Murty,V.V. and Benezra,R. (2001) MAD2 haplo-insufficiency causes premature anaphase and chromosome instability in mammalian cells. *Nature*, **409**, 355–359.
21. Miyagawa,K., Tsuruga,T., Kinomura,A., Usui,K., Katsura,M., Tashiro,S., Mishima,H. and Tanaka,K. (2002) A role for *RAD54B* in homologous recombination in human cells. *EMBO J.*, **21**, 175–180.
22. Yoshihara,T., Ishida,M., Kinomura,A., Katsura,M., Tsuruga,T., Tashiro,S., Asahara,T. and Miyagawa,K. (2004) XRCC3 deficiency results in a defect in recombination and increased endoreduplication in human cells. *EMBO J.*, **23**, 670–680.
23. Wassmann,K. and Benezra,R. (1998) Mad2 transiently associates with an APC/p55Cdc complex during mitosis. *Proc. Natl Acad. Sci. USA*, **95**, 11193–11198.
24. Gao,H., Chen,X.-B. and McGowan,C.H. (2003) Mus81 endonuclease localizes to nucleoli and to regions of DNA damage in human S phase cells. *Mol. Biol. Cell*, **14**, 4826–4834.
25. Tashiro,S., Walter,J., Shinohara,A., Kamada,N. and Cremer,T. (2000) Rad51 accumulation at sites of DNA damage and in postreplicative chromatin. *J. Cell. Biol.*, **150**, 283–291.

26. Bishop,D.K., Ear,U., Bhattacharyya,A., Calderone,C., Beckett,M., Weichselbaum,R.R. and Shinohara,A. (1998) Xrcc3 is required for assembly of Rad51 complexes *in vivo*. *J. Biol. Chem.*, **273**, 21482–21488.
27. Takata,M., Sasaki,M.S., Tachiiri,S., Fukushima,T., Sonoda,E., Schild,D., Thompson,L.H. and Takeda,S. (2001) Chromosome instability and defective recombinational repair in knockout mutants of the five Rad51 paralogs. *Mol. Cell. Biol.*, **21**, 2858–2866.
28. Solinger,J.A., Kiianitsa,K. and Heyer,W.-D. (2002) Rad54, a Swi2/Snf2-like recombinational repair protein, disassembles Rad51:dsDNA filaments. *Mol. Cell*, **10**, 1175–1188.
29. Tan,T.L.R., Essers,J., Citterio,E., Swagemakers,S.M.A., de Wit,J., Benson,F.E., Hoeijmakers,J.H.J. and Kanaar,R. (1999) Mouse Rad54 affects DNA conformation and DNA-damage-induced Rad51 foci formation. *Curr. Biol.*, **9**, 325–328.
30. Thompson,L.H. and Schild,D. (2001) Homologous recombinational repair of DNA ensures mammalian chromosome stability. *Mutat. Res.*, **477**, 131–153.
31. Bartek,J., Lukas,C. and Lukas,J. (2004) Checking on DNA damage in S phase. *Nature Rev. Mol. Cell Biol.*, **5**, 792–804.
32. Sorensen,C.S., Syljuasen,R.G., Falck,J., Schroeder,T., Ronnstrand,L., Khanna,K.K., Zhou,B.-B., Bartek,J. and Lukas,J. (2003) Chk1 regulates the S phase checkpoint by coupling the physiological turnover and ionizing radiation-induced accelerated proteolysis of Cdc25A. *Cancer Cell*, **3**, 247–258.
33. Falck,J., Mailand,N., Syljuasen,R.G., Bartek,J. and Lukas,J. (2001) The ATM-Chk2-Cdc25A checkpoint pathway guards against radioresistant DNA synthesis. *Nature*, **410**, 842–847.
34. Shen,M., Feng,Y., Gao,C., Tao,D., Hu,J., Reed,E., Li,Q.Q. and Gong,J. (2004) Detection of cyclin B1 expression in G_1 phase cancer cell lines and cancer tissues by postsorting western blot analysis. *Cancer Res.*, **64**, 1607–1610.
35. Iliakis,G., Wang,Y., Guan,J. and Wang,H. (2003) DNA damage checkpoint control in cells exposed to ionizing radiation. *Oncogene*, **22**, 5834–5847.
36. Matsuoka,S., Huang,M. and Elledge,S.J. (1998) Linkage of ATM to cell cycle regulation by the Chk2 protein kinase. *Science*, **282**, 1893–1897.
37. Kaufmann,W.K., Heffernan,T.P., Beaulieu,L.M., Doherty,S., Frank,A.R., Zhou,Y., Bryant,M.F., Zhou,T., Luche,D.D., Nikolaishvili-Feinberg,N. *et al.* (2003) Caffeine and human DNA metabolism: the magic and the mystery. *Mutat. Res.*, **532**, 85–102.
38. Blasina,A., Price,B.D., Turenne,G.A. and McGowan,C.H. (1999) Caffeine inhibits the checkpoint kinase ATM. *Curr. Biol.*, **9**, 1135–1138.
39. Sarkaria,J.N., Busby,E.C., Tibbetts,R.S., Roos,P., Taya,Y., Karnitz,L.M. and Abraham,R.T. (1999) Inhibition of ATM and ATR kinase activities by the radiosensitizing agent, caffeine. *Cancer Res.*, **59**, 4375–4382.
40. Zhou,B.-B.S., Chaturvedi,P., Spring,K., Scott,S.P., Johanson,R.A., Mishra,R., Mattern,M.R., Winkler,J.D. and Khanna,K.K. (2000) Caffeine abolishes the mammalian G_2/M DNA damage checkpoint by inhibiting ataxia-telangiectasia-mutated kinase activity. *J. Biol. Chem.*, **275**, 10342–10348.
41. Lukas,J., Lukas,C. and Bartek,J. (2004) Mammalian cell cycle checkpoints: signaling pathways and their organization in space and time. *DNA Repair*, **3**, 997–1007.
42. Itzhaki,J.E., Gilbert,C.S. and Porter,A.C.G. (1997) Construction by gene targeting in human cells of a 'conditional' *CDC2* mutant that rereplicates its DNA. *Nature Genet.*, **15**, 258–265.
43. Constantinou,A., Chen,X.-B., McGowan,C.H. and West,S.C. (2002) Holliday junction resolution in human cells: two junction endonucleases with distinct substrate specificities. *EMBO J.*, **21**, 5577–5585.
44. Liu,Y., Masson,J.-Y., Shah,R., O'Regan,P. and West,S.C. (2004) RAD51C is required for Holliday junction processing in mammalian cells. *Science*, **303**, 243–246.
45. Bastin-Shanower,S.A., Fricke,W.M., Mullen,J.R. and Brill,S.J. (2003) The mechanism of Mus81-Mms4 cleavage site selection distinguishes it from the homologous endonuclease Rad1-Rad10. *Mol. Cell. Biol.*, **23**, 3487–3496.
46. Fabre,F., Chan,A., Heyer,W.-D. and Gangloff,S. (2002) Alternate pathways involving Sgs1/Top3, Mus81/Mms4, and Srs2 prevent formation of toxic recombination intermediates from single-stranded gaps created by DNA replication. *Proc. Natl Acad. Sci. USA*, **99**, 16887–16892.
47. Doe,C.L., Osman,F., Dixon,J. and Whitby,M.C. (2004) DNA repair by a Rad22-Mus81-dependent pathway that is independent of Rhp51. *Nucleic Acids Res.*, **32**, 5570–5581.
48. Abraham,R.T. (2001) Cell cycle checkpoint signaling through the ATM and ATR kinases. *Genes Dev.*, **15**, 2177–2196.
49. Nguyen,V.Q., Co,C. and Li,J.J. (2001) Cyclin-dependent kinases prevent DNA re-replication through multiple mechanisms. *Nature*, **411**, 1068–1073.
50. Wuarin,J., Buck,V., Nurse,P. and Millar,J.B.A. (2002) Stable association of mitotic Cyclin B/Cdc2 to replication origins prevents endoreduplication. *Cell*, **111**, 419–431.
51. Fujiwara,T., Bandi,M., Nitta,M., Ivanova,E.V., Bronson,R.T. and Pellman,D. (2005) Cytokinesis failure generating tetraploids promotes tumorigenesis in *p53*-null cells. *Nature*, **437**, 1043–1047.
52. Shi,Q. and King,R.W. (2005) Chromosome nondisjunction yields tetraploid rather than aneuploid cells in human cell lines. *Nature*, **437**, 1038–1042.

Available online at www.sciencedirect.com
SCIENCE DIRECT
ELSEVIER
Biochemical and Biophysical Research Communications 341 (2006) 363–368
BBRC
www.elsevier.com/locate/ybbrc

Src tyrosine kinase inhibitor PP2 suppresses ERK1/2 activation and epidermal growth factor receptor transactivation by X-irradiation

Zhiping Li [a], Yoshio Hosoi [a,*], Keshong Cai [a], Yuji Tanno [a], Yoshihisa Matsumoto [a], Atsushi Enomoto [a], Akinori Morita [a], Keiichi Nakagawa [b], Kiyoshi Miyagawa [a]

[a] *Department of Radiation Research, Faculty of Medicine, University of Tokyo, Tokyo 113-0033, Japan*
[b] *Department of Radiology, Faculty of Medicine, University of Tokyo, Tokyo 113-0033, Japan*

Received 26 December 2005
Available online 18 January 2006

Abstract

Exposure of MDA-MB-468 cells to ionizing radiation (IR) caused biphasic activation of ERK as indicated by its phosphorylation at Thr202/Tyr204. Specific epidermal growth factor receptor (EGFR) inhibitor AG1478 and specific Src inhibitor PP2 inhibited IR-induced ERK1/2 activation but phosphatidylinositol-3 kinase inhibitor wortmannin did not. IR caused EGFR tyrosine phosphorylation, whereas it did not induce EGFR autophosphorylation at Tyr992, Tyr1045, and Tyr1068 or Src-dependent EGFR phosphorylation at Tyr845. SHP-2, which positively regulates EGFR/Ras/ERK signaling cascade, became activated by IR as indicated by its phosphorylation at Tyr542. This activation was inhibited by PP2 not by AG1478, which suggests Src-dependent activation of SHP-2. Src and PTPα, which positively regulates Src, became activated as indicated by phosphorylation at Tyr416 and Tyr789, respectively. These data suggest that IR-induced ERK1/2 activation involves EGFR through a Src-dependent pathway that is distinct from EGFR ligand activation.

Keywords: Ionizing radiation; EGFR; Src; Transactivation; ERK; SHP-2; PP2; AG1478

Ionizing radiation (IR) has been shown to activate epidermal growth factor receptor (EGFR) and extracellular signal-regulated kinase (ERK) [1–3]. EGFR activation by IR initiates the Ras/Raf/ERK signaling cascade, stimulates cell proliferation, and leads cells to be resistant to IR [1–5]. The molecular mechanisms underlying IR-induced activation of EGFR are not clear. One of the possible mechanisms is activation of Src. IR induces production of hydrogen peroxide. Treatment with hydrogen peroxide activates Src, and specific EGFR inhibitor AG1478, and specific Src inhibitors PP1 and PP2 inhibit the activation of EGFR and ERK1/2 induced by hydrogen peroxide [6–9]. Ultraviolet (UV) radiation induces intracellular production of hydrogen peroxide and causes activation of EGFR and ERK1/2 [10]. Both AG1478 and PP2 block the UV-induced activation of EGFR and ERK1/2 [11]. These results indicate the fundamental role of Src in the activation of EGFR and ERK1/2 following treatment with hydrogen peroxide and UV.

We considered the possibility that IR-induced intracellular hydrogen peroxide caused activation of EGFR and ERK1/2 through Src activation just as hydrogen peroxide and UV did. To investigate this, we studied the effects of IR on activities of ERK1/2, EGFR, SHP-2, Src, and PTPα as indicated by their tyrosine phosphorylation and effects of AG1478 and PP2 on them. In this report, we show IR-induced activation of ERK1/2, SHP-2, Src, and PTPα, and inhibition of IR-induced activation of ERK1/2 and SHP-2 by AG1478 and PP2, which suggests that IR-induced ERK1/2 activation is mediated through activation of Src/SHP-2 and EGFR.

Materials and methods

Reagents. Recombinant human epidermal growth factor (EGF) was purchased from Wako Pure Chemical Industries (Osaka, Japan). AG1478

* Corresponding author. Fax: +81 3 5841 3013.
E-mail address: hosoi@m.u-tokyo.ac.jp (Y. Hosoi).

0006-291X/$ - see front matter © 2006 Elsevier Inc. All rights reserved.
doi:10.1016/j.bbrc.2005.12.193

and PP2 were obtained from Calbiochem (La Jolla, CA). Wortmannin was obtained from Sigma–Aldrich (St. Louis, MO). Anti-phospho-ERK1/2 (Thr202/Tyr204), anti-ERK1/2, anti-phospho-EGFR (Tyr845, Tyr992, Tyr1045, and Tyr1068), anti-phospho-SHP-2 (Tyr542), anti-SHP-2, anti-phospho-Src (Tyr416), and anti-phospho-PTPα (Tyr789) antibodies were purchased from Cell Signaling Technology (Beverly, MA). Anti-Src antibody was from Oncogene Research Products (San Diego, CA). Anti-EGFR antibody was from Transduction Laboratories (Lexington, KY). Anti-β-actin antibody was from Sigma (St. Louis, MO). A human breast cancer cell line MDA-MB-468 was obtained from American Type Culture Collection (Rockville, MD).

Cell culture, irradiation, and EGF treatment. Cells were cultured at 37 °C, 5% CO_2 in minimum essential medium (MEM) containing 10% fetal calf serum. Cells were plated at 5×10^5 cells in 60-mm dishes and incubated for 4 days without changing the culture medium. Cells were then treated with X-irradiation (200 kV, 20 mA, 0.5 mm Cu, and 1.0 mm Al filters, 1.36 Gy/min: HF-350C, SHIMADZU, Kyoto, Japan) or 10 ng/ml EGF. Cells were incubated at 37 °C for up to 6 h post the treatment and lysates were subjected to immunoblotting.

Immunoblotting. Cells were lysed in the electrophoresis sample buffer (62.5 mM Tris (pH 6.8), 2% SDS, 5% glycerol, 0.003% bromophenol blue, and 1% β-mercaptoethanol) and boiled for 5 min. The cell lysate was resolved by 7.5% polyacrylamide gel electrophoresis and was electrophoretically transferred to polyvinylidene difluoride membranes (Millipore, Bedford, MA). The membranes were then proved with antibodies and the antigen–antibody complexes were detected by the ECL Plus Western blotting detection reagents (Amersham Pharmacia Biotech, Piscataway, NJ) with horseradish peroxidase-conjugated antibodies.

Immunoprecipitation. Cells were washed with ice-cold Tris-buffered saline twice and incubated in lysis buffer (20 mM Hepes (pH 7.4), 150 mM NaCl, 1 mM EDTA, 1 mM EGTA, 1.0% Triton X-100, 0.5% deoxycholate (sodium salt), 1 mM sodium orthovanadate, 1 mM PMSF, and 1 μg/ml leupeptin) for 20 min on ice. Cell lysates were then centrifuged at 13,500*g* for 10 min, the supernatants were incubated with protein G–Sepharose with primary antibody for 2 h. Following brief centrifugation, pellets were washed four times with lysis buffer and resuspended in loading buffer (125 mM Tris (pH 6.8), 4% SDS, 10% glycerol, 0.006% bromophenol blue, and 2% β-mercaptoethanol).

Results

Activation of ERK1/2 by ionizing radiation

First, we examined the effects of IR on ERK1/2 activity as indicated by its phosphorylation at Thr202/Tyr204. Irradiation with 0.5, 2, and 10 Gy caused an immediate ERK1/2 activation observed 2–5 min after irradiation followed by a late activation observed 6 h after irradiation (Fig. 1A). We further investigated the effects of IR on ERK1/2 activity with a wider dose range and found that irradiation with 0.1–20 Gy induced ERK1/2 activation (Fig. 1B).

Effects of AG1478, PP2, and wortmannin on IR-induced ERK1/2 activation

To investigate the signal transduction pathway involving IR-induced ERK1/2 activation, we studied effects of specific EGFR inhibitor AG1478 and specific Src inhibitor PP2 on IR-induced ERK1/2 activation. We first examined effects of AG1478 and PP2 on EGF-induced ERK1/2 activation to compare the IR-induced EGFR activation with the ligand-dependent one. AG1478 suppressed

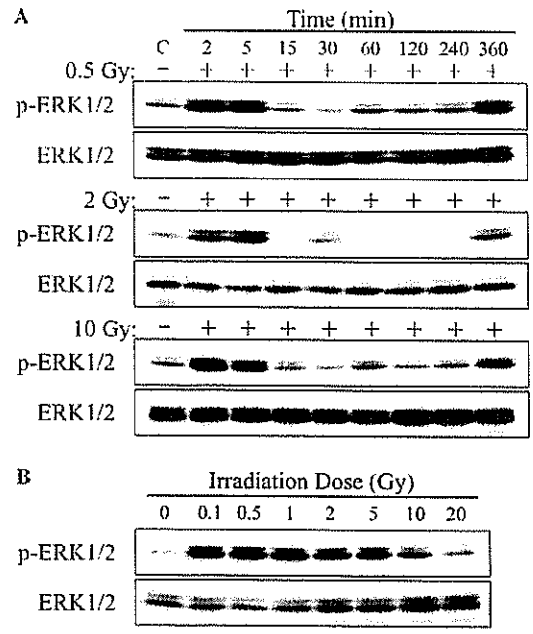

Fig. 1. ERK1/2 becomes phosphorylated at Thr202/Tyr204 in response to 0.1–20 Gy irradiation. (A) MDA-MB-468 cells were irradiated with 0.5, 2.0 or 10 Gy and incubated for 2–360 min at 37 °C. Whole cell lysates were then prepared and immunoblotted for phospho-ERK1/2 (Thr202/Tyr204) and ERK1/2. (B) MDA-MB-468 cells were irradiated with 0.1–20 Gy and incubated for 2 min at 37 °C. Whole cell lysates were then prepared and immunoblotted similarly.

EGF-induced ERK1/2 activation at 2–5 min after the addition of EGF into the culture medium but it failed to suppress the ERK1/2 activation later (Fig. 2A). PP2 did not suppress EGF-induced ERK1/2 activation (Fig. 2A). These results suggest that EGF-induced ERK1/2 activation is independent of Src. Next, we examined effects of AG1478 and PP2 on IR-induced ERK1/2 activation. AG1478 suppressed IR-induced ERK1/2 activation (Fig. 2B). PP2 suppressed the ERK1/2 activation observed 2–5 min after irradiation and partially suppressed the activation observed 360 min after irradiation (Fig. 2B). Although ERK1/2 activation has been linked to the activity of phosphatidylinositol-3 kinase (PI3K) in some system [12], we did not observe effects of PI3K-inhibition with wortmannin on IR-induced ERK1/2 activation (Fig. 2B). These results suggest that IR-induced ERK1/2 activation observed 2-5 min after irradiation is mediated by EGFR and Src.

IR-induced tyrosine phosphorylation of EGFR

Irradiation with 2 Gy induced immediate tyrosine phosphorylation observed 2–5 min after irradiation followed by a late tyrosine phosphorylation observed 6 h after irradiation (Fig. 3A). This time course of tyrosine phosphorylation corresponds to that of IR-induced ERK1/2 activation (Fig. 1A).

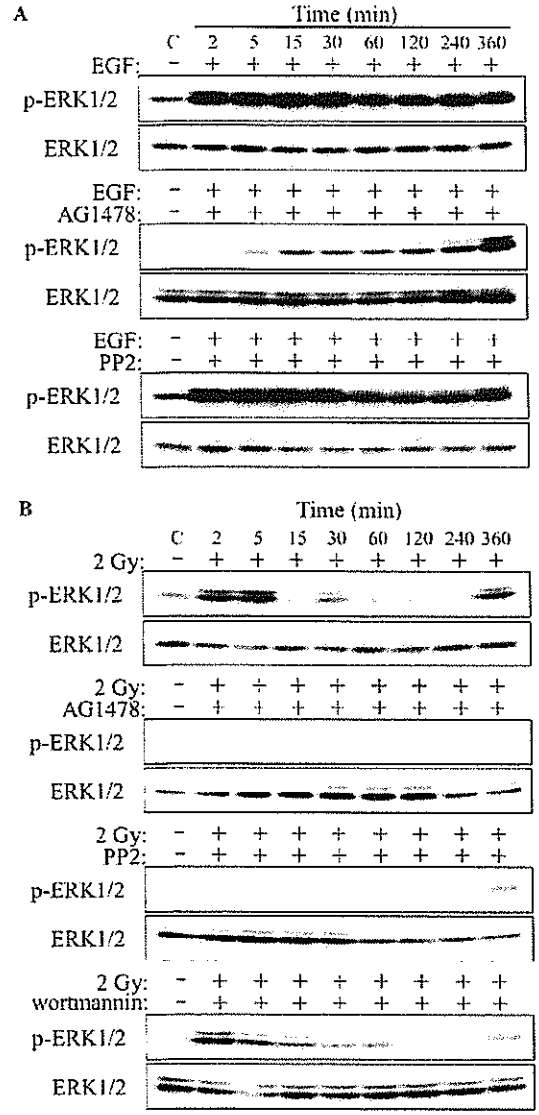

Fig. 2. Effects of AG1478, PP2 and wortmannin on ERK1/2 activation induced by EGF treatment or 2 Gy irradiation. MDA-MB-468 cells were treated with 0.5 μM AG1478, 10 μM PP2 or 200 nM wortmannin 30 min before the treatment with 10 ng/ml EGF (A) or 2 Gy irradiation (B). After the treatment with EGF or irradiation, cells were incubated for 2–360 min at 37 °C. Whole cell lysates were then prepared and immunoblotted for phospho-ERK1/2 (Thr202/Tyr204) and ERK1/2.

Effects of IR on EGFR phosphorylation at Tyr845, Tyr992, Tyr1045, and Tyr1068

For further investigation of EGFR phosphorylation after exposure to IR, we investigated IR-induced EGFR phosphorylation at Tyr845, Tyr992, Tyr1045, and Tyr1068 using antibodies specific to these phosphorylation sites of the activated EGFR. The phosphorylation at Tyr992, Tyr1045, and Tyr1068 has been reported to be mediated by EGFR tyrosine kinase and the phosphorylation at

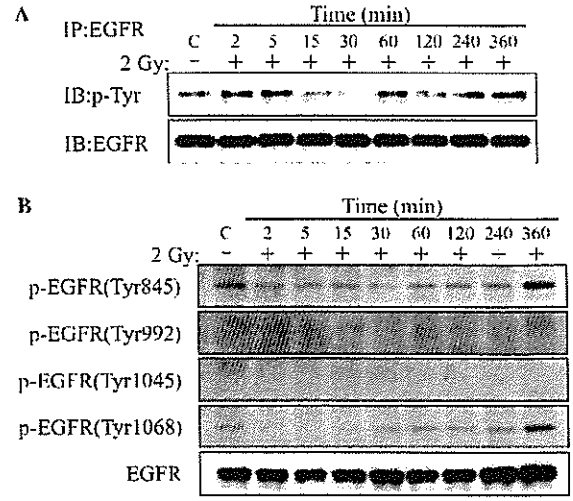

Fig. 3. Effects of IR on tyrosine phosphorylation of EGFR. MDA-MB-468 cells were irradiated with 2 Gy. After irradiation, cells were incubated for 2–360 min at 37 °C. Whole cell lysates were then prepared. (A) The whole cell lysates were subjected to immunoprecipitation with anti-EGFR antibody. The immunoprecipitates were immunoblotted for phosphotyrosine (p-Tyr) and EGFR. (B) The whole cell lysates were immunoblotted for phospho-EGFR (Tyr845, Tyr992, Tyr1045, and Tyr1068) and EGFR.

Tyr845 by Src [13,14]. Irradiation with 2 Gy caused a prompt decrease of EGFR phosphorylation at Tyr845 and Tyr1068 observed 2–15 min after irradiation followed by an increase of the phosphorylation observed 6 h after irradiation without obvious alteration of the phosphorylation at Tyr992 and Tyr1045 (Fig. 3B). In response to EGF stimulation, EGFR became phosphorylated at Tyr845, Tyr1068 (Fig. 4A), Tyr992, and Tyr1045 (data not shown). These data indicate that IR-mediated ERK1/2 activation involves an autophosphorylation-independent mechanism that is distinct from EGFR ligand activation.

Effects of AG1478 and PP2 on EGFR phosphorylation after EGF treatment or 2 Gy irradiation

Because EGFR phosphorylation at Tyr845 and Tyr1068 was affected by IR (Fig. 3B), we investigated effects of AG1478 and PP2 on EGF- and IR-induced phosphorylation at Tyr845 and Tyr1068 [13,14]. AG1478 partially suppressed EGF-induced phosphorylation and it suppressed IR-induced phosphorylation observed 6 h after irradiation (Figs. 4A and B). PP2 suppressed EGF- and IR-induced phosphorylation at Tyr845 but it failed to suppress the phosphorylation at Tyr1068 (Figs. 4A and B).

Irradiation with 2 Gy induces SHP-2 activation, which is inhibited by PP2

SHP-2 positively regulates the ability of several receptor tyrosine kinases (RTKs) to activate the Ras/Raf/ERK signaling cascade, and it plays a fundamental role in the regulation of Ras/Raf/ERK signaling from RTKs [15,16]. We

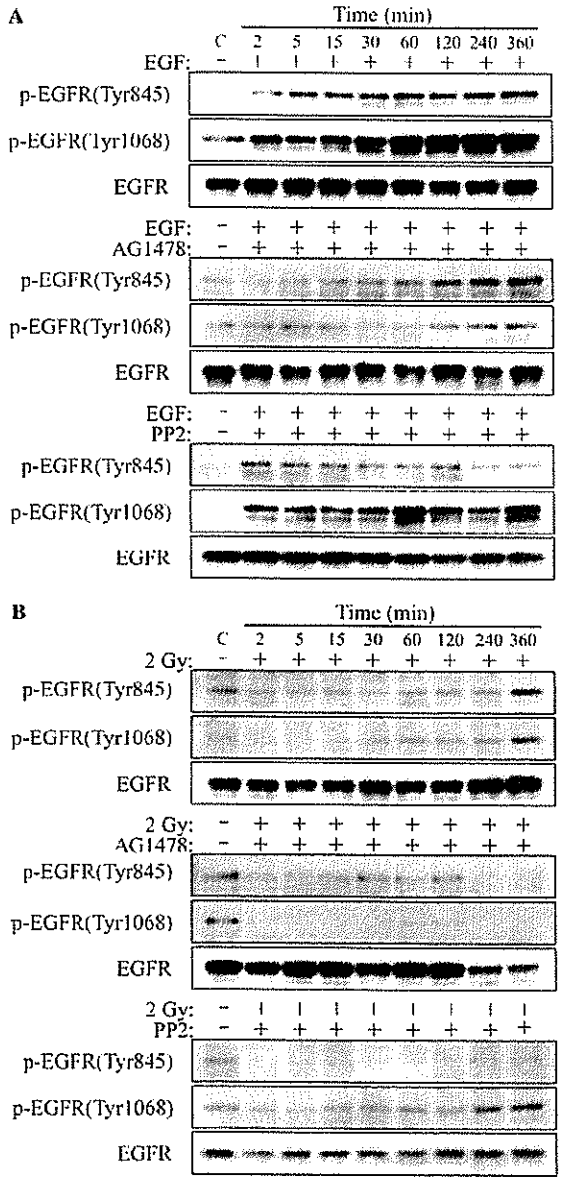

Fig. 4. Effects of AG1478 and PP2 on the phosphorylation status of EGFR after EGF treatment or 2 Gy irradiation. MDA-MB-468 cells were treated with 0.5 μM AG1478 or 10 μM PP2 30 min before the treatment with 10 ng/ml EGF (A) or 2 Gy irradiation (B). After the treatment with EGF or irradiation, cells were incubated for 2–360 min at 37 °C. Whole cell lysates were then prepared and immunoblotted for phospho-EGFR (Tyr845, Tyr1068) and EGFR.

examined if IR affected SHP-2 activity because Src and RTKs activate SHP-2 [16–18]. We first examined the effects of EGF on SHP-2 activity and found that SHP-2 became activated after EGF treatment as indicated by its phosphorylation at Tyr542 (Fig. 5A). AG1478 little affected EGF-induced phosphorylation of SHP-2, whereas PP2 suppressed the increased phosphorylation (Fig. 5A). These data indicate that EGF-induced SHP-2 activation is mainly

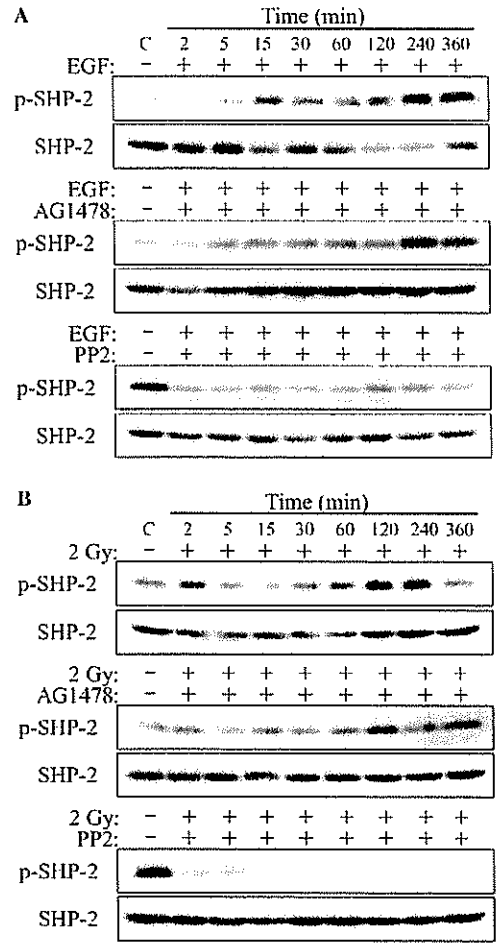

Fig. 5. SHP-2 becomes phosphorylated in response to 2 Gy irradiation and EGF, which is inhibited by PP2 and AG1478. MDA-MB-468 cells were treated with 0.5 μM AG1478 or 10 μM PP2 30 min before the treatment with 10 ng/ml EGF (A) or 2 Gy irradiation (B). After the treatment with EGF or irradiation, cells were incubated for 2–360 min at 37 °C. Whole cell lysates were then prepared and immunoblotted for phospho-SHP-2 (Tyr542) and SHP-2.

mediated by Src. Next, we examined effect of IR on SHP-2 activity. IR caused increased SHP-2 phosphorylation 2 min and 1–6 h after irradiation (Fig. 5B). This enhanced phosphorylation was little affected by AG1478 and suppressed by PP2, which suggests that IR-induced SHP-2 activation is also mediated by Src (Fig. 5B).

IR induces activation of Src and PTPα

Since PP2 inhibited IR-induced ERK1/2 and SHP-2 activation (Figs. 2B and 4B), we examined effects of IR on Src. Src became activated 1–6 h after 2 Gy irradiation as indicated by its phosphorylation at Tyr416 (Fig. 6). Next, we investigated the effect of IR on the activity of PTPα that activates Src by dephosphorylation at Tyr527 [19]. PTPα became activated 1–6 h after 2 Gy irradiation as indicated by its phosphorylation at Tyr789 (Fig. 6).